PHYSICAL REVIEW D **81,** 084016 (2010)

Effective one body description of tidal effects in inspiralling compact binaries

Thibault Damour and Alessandro Nagar

Institut des Hautes Etudes Scientifiques, 91440 Bures-sur-Yvette, France and ICRANet, 65122 Pescara, Italy

(Received 26 November 2009; published 8 April 2010)

The late part of the gravitational wave signal of binary neutron-star (or black-hole–neutron-star) inspirals can in principle yield crucial information on the nuclear equation of state via its dependence on relativistic tidal parameters. In the hope of analytically describing the gravitational wave phasing during the late inspiral (essentially up to merger) we propose an extension of the effective one body (EOB) formalism which includes tidal effects. We compare the prediction of this tidal-EOB formalism to recently computed nonconformally flat quasiequilibrium circular sequences of binary neutron-star systems. Our analysis suggests the importance of higher-order (post-Newtonian) corrections to tidal effects, even beyond the first post-Newtonian order, and their tendency to *significantly increase* the ''effective tidal polarizability'' of neutron stars. We propose to use the EOB description up to the moment where the tidally deformed compact objects formally enter ''into contact.'' We compare the EOB predictions to some recently advocated, nonresummed, post-Newtonian based (''Taylor-T4'') description of the phasing of inspiralling systems. This comparison shows the strong sensitivity of the late-inspiral phasing to the choice of the analytical model. A sufficiently accurate numerical–relativity–''calibrated'' EOB model might, however, give us a reliable analytical description of the late inspiral of compact binaries (and might also help in predicting the conditions necessary for the generation of short gamma-ray bursts).

DOI: 10.1103/PhysRevD.81.084016 PACS numbers: 04.25.Nx, 04.30.−w, 04.40.Dg

I. INTRODUCTION

Some of the prime targets of the currently operating network of ground-based detectors of gravitational waves (GWs) are the signals emitted by inspiralling and coalescing compact binaries. Here, compact binary refers to a binary system made either of two black holes, a black hole and a neutron star, or two neutron stars. The GW signal emitted by binary black-hole (BBH) systems has been the subject of intense theoretical studies, based either on analytical methods or on numerical ones. In particular, recent progress in the application of the effective one body (EOB) approach to BBH systems has led to a remarkable agreement between the (analytical) EOB predictions and the best current numerical relativity (NR) results [1,2] (see also [3]). By contrast, much less work has been devoted to the study of the GW signal emitted by compact binaries comprising neutron stars: either black-hole–neutron-star (BHNS) systems or binary neutron-star (BNS) ones. During the inspiral phase (before merger), these systems differ from the BBH ones by the presence of tidal interactions which affect both the dynamics of the inspiral and the emitted waveform. During the merger and coalescence phase, the presence of neutron stars drastically modifies the GW signal [4–6]. The coalescence signal involves (especially in the BNS case) a lot of complicated physics and astrophysics, and is, probably, not amenable to the type of accurate analytical description which worked in the BBH case. Early works on this problem have tried to approximately relate some qualitative features of the merger GW signal linked, e.g., to tidal disruption, to analytically describable inputs [7–9].

Recently, Flanagan and Hinderer [10–12] initiated the program of studying the quantitative influence of tidal effects [11,13,14] in inspiralling BNS systems. However, they only considered the early (lower-frequency) portion of the GW inspiral signal, mainly because they were using a post-Newtonian (PN) based description of the binary dynamics whose validity is restricted to low enough frequencies. In particular, one of the results of the recent work of Hinderer *et al.* [12] is to show that the accumulated GW phase due to tidal interactions is, for most realistic NS models of mass $M \sim 1.4M_\odot$ *smaller* than the uncertainty in the PN-based description of GW phasing (see the central panel of Fig. 4 in Ref. [12] where the thin-dashed and thin-dotted lines are two measures of the PN uncertainty). (These measures are larger than the inspiral tidal signal except for the extreme case where the radius of the $1.4M_\odot$ NS is taken to be ≥ 16 km.)

By contrast, our aim in this work is to propose a way of describing the binary dynamics (including tidal effects) whose validity does not have the limitations of PN-based descriptions and therefore is not *a priori* limited to the low-frequency part, but extends to significantly higher frequencies. This might be crucial to increase the detectability of the GW signal and thereby have a handle on the nuclear equation of state (EOS). Indeed, our proposal consists in extending the EOB method by incorporating tidal effects in it. Our hope is that such a tidally extended EOB framework will be able to describe with sufficient approximation not only the early inspiral phase, but also the late inspiral up to the moment (that we shall consistently determine within our scheme) of ''contact.'' As we shall indicate, such a framework might also give us an analytic handle on the

possible formation of hot disks around merging systems. We think that the present EOB description of tidal effects is likely to be more accurate than any of the possible post-Newtonian-based descriptions involving supplementary tidal terms (such as [10] or [12]). This should be especially true in the BHNS systems which, in the limiting case $m_{\rm NS} \ll m_{\rm BH}$, are known to be well described by the EOB approach (and rather badly described by post-Newtonian-based approaches). We will give some evidence of the validity of the EOB description of close neutron-star systems by comparing our analytical predictions to recently calculated quasiequilibrium NS sequences of circular orbits [15] (see also [16]).

II. EFFECTIVE-ACTION DESCRIPTION OF TIDAL EFFECTS IN TWO BODY SYSTEMS

A. General formalism

The general relativistic tidal properties of neutron stars have been recently studied in Refs. [11–14]. As emphasized in [13], there are (at least) three different types of tidal responses of a neutron star to an external tidal solicitation, which are measured by three different tidal coefficients: (i) a gravito-electric-type coefficient $G\mu_\ell = [\text{length}]^{2\ell+1}$ measuring the ℓth-order mass multipolar moment $GM_{a_1\cdots a_\ell}$ induced in a star by an external ℓth-order gravito-electric tidal field $G_{a_1\cdots a_\ell}$; (ii) a gravitomagnetic-type coefficient $G\sigma_\ell = [\text{length}]^{2\ell+1}$ measuring the ℓth spin multipole moment $GS_{a_1\cdots a_\ell}$ induced in a star by an external ℓth-order gravitomagnetic tidal field $H_{a_1\cdots a_\ell}$; and (iii) a dimensionless shape Love number h_ℓ measuring the distortion of the shape of the surface of a star by an external ℓth-order gravito-electric tidal field. It was found in [13,14] that all those coefficients have a strong sensitivity to the value of the star's compactness $c \equiv GM/c_0^2R$ (where we denote by c_0 the velocity of light,[1] to be distinguished from the compactness c). This means, in particular, that the numerical values of the tidal coefficients of NS's should not be evaluated by using Newtonian estimates. Indeed, the dimensionless version of μ_ℓ, traditionally denoted as k_ℓ (second Love number) and defined as

$$2k_\ell \equiv (2\ell-1)!!\frac{G\mu_\ell}{R^{2\ell+1}}, \tag{1}$$

where R denotes the areal radius of the NS, is typically 3 times smaller than its Newtonian counterpart (computed from the same equation of state). A similar, though less drastic, quenching also occurs for the first Love number h_ℓ. In particular, though Newtonian h_ℓ's are larger than 1 [and equal to $1 + 2k_\ell$, see Eq. (81) of [13]], the typical relativistic values of h_ℓ are smaller than 1. This will play a useful role in our analysis below of the moment where the tidal distortion of the NS becomes too large for continuing to use an analytical approach.

It was shown in [17,18] that the motion and radiation of two black holes can be described, up to the fifth post-Newtonian (5PN) approximation, by an effective action of the form

$$S_0 = \int \frac{d^Dx}{c_0}\frac{c_0^4}{16\pi G}\sqrt{g}R(g) + S_{\text{point mass}}, \tag{2}$$

where

$$S_{\text{point mass}} = -\sum_A \int M_A c_0^2 ds_A, \tag{3}$$

is a skeletonized description of black holes, as point masses. Here ds_A denotes the proper time along the worldline of A normalized as $ds_A = c_0^{-1}(-g_{\mu\nu}(z_A)dz_A^\mu dz_A^\nu)^{1/2}$.

To give meaning to the addition of point-mass sources to the nonlinear Einstein equations, one needs to use a covariant regularization method. References [17,18] mainly used Riesz's analytic regularization, but it was already mentioned at the time that one could equivalently use dimensional regularization. The efficiency and consistency of the latter method was shown by the calculations of the dynamics, and radiation, of BBH systems at the 3PN level [19–21]. Let us also recall that the limitation to the 5PN level in Ref. [18] is precisely linked to the possible appearance of ambiguities in BBH dynamics appearing at the level where tidal effects start entering the picture. Indeed, it is well known in effective field theory that finite-size effects correspond to augmenting the point-mass action (2) by nonminimal (worldline) couplings involving higher-order derivatives of the field (see [22,23] and Appendix A of Ref. [24]). More precisely, the two tidal effects parametrized by μ_ℓ and σ_ℓ correspond to augmenting the leading point-particle effective action, (2) and (3), by the following nonminimal worldline couplings:

$$\Delta S_{\text{nonminimal}} = \sum_A \Big\{ \frac{1}{2}\frac{1}{\ell!}\mu_\ell^A \int ds_A (G_L^A)^2 + \frac{1}{2}\frac{\ell}{\ell+1}\frac{1}{\ell!} \times \frac{1}{c_0^2}\sigma_\ell^A \int ds_A (H_L^A)^2 \Big\}. \tag{4}$$

Here[2] $G_L^A \equiv G^A_{a_1\cdots a_\ell}$ and $H_L^A \equiv H^A_{a_1\cdots a_\ell}$ are the gravito-electric and gravito-magnetic external tidal gradients evaluated along the worldline of the considered star (labeled by A), in the local frames (attached to body A) defined in [25]. If needed, they can be reexpressed in terms of covariant derivatives of the Riemann (or Weyl) tensor. For instance, using Eq. (3.40) of [25], the leading, quadrupolar terms in Eq. (4) read

[1] In the following, we will often set the velocity of light $c_0 = 1$ when it is not useful to keep track of the PN order.

[2] We use here the notation of [25], notably for multi-indices $L \equiv a_1 \cdots a_\ell$.

$$\Delta S_{\rm nonminimal} = \sum_A \Big\{ \frac{1}{4}\mu_2^A \int ds_A \mathcal{E}^A_{\alpha\beta}\mathcal{E}^{A_{\alpha\beta}} + \frac{1}{6}\sigma_2^A \int ds_A \mathcal{B}^A_{\alpha\beta}\mathcal{B}^{A_{\alpha\beta}} + \cdots \Big\}, \quad (5)$$

where $\mathcal{E}^A_{\alpha\beta} \equiv [u^\mu u^\nu C_{\mu\alpha\nu\beta}]^A$, $\mathcal{B}^A_{\alpha\beta} \equiv [u^\mu u^\nu C^*_{\mu\alpha\nu\beta}]^A$, with $C^*_{\mu\nu\alpha\beta} \equiv \frac{1}{2}\epsilon_{\mu\nu\rho\sigma}C^{\rho\sigma}{}_{\alpha\beta}$ being the dual of the Weyl tensor C, and $u^\mu = dz^\mu/ds$ ($u^2 = -c_0^2$) being the four-velocity along the considered worldline. As explained in Appendix A of Ref. [24], one can, modulo some suitable field redefinitions that do not affect the leading result, indifferently use the Weyl tensor $C_{\alpha\beta\mu\nu}$ or the Riemann tensor $R_{\alpha\beta\mu\nu}$ in evaluating the $\mathcal{E}_{\alpha\beta}$ and $\mathcal{B}_{\alpha\beta}$ entering Eq. (5).

The effective-action terms (4) and (5) can be used to compute the various observable effects linked to the relativistic tidal coefficients μ_ℓ and σ_ℓ.[3] In particular, they imply both (i) additional terms in the dynamics of the considered binary system, and (ii) additional terms in the gravitational radiation emitted by the considered binary system. Both types of additional terms can, in principle, be evaluated with any needed relativistic accuracy from Eq. (4), i.e. computed either in a post-Minkowskian (PM) expansion in powers of G/c_0^2, or (after a further reexpansion in powers of $1/c_0$), in a post-Newtonian (PN) expansion in powers of $1/c_0^2$. Let us remark in passing that the PM expansion can be conveniently expressed in terms of Feynman-like diagrams, as was explicitly discussed (for tensor-scalar gravity) at the 2PN level in [22].

Here we shall use the extra terms (4) and (5) as a way to *add* to the description of binary black-hole systems the effects linked to the replacement of one or two of the black holes by a neutron star. From this point of view, we shall conventionally consider that the tidal coefficients of a black hole vanish: $\mu_\ell^{\rm BH} = 0 = \sigma_\ell^{\rm BH}$ [13,14]. However, as emphasized in [13], more work is needed to clarify whether this is exact, i.e. whether the description of BBH's by an effective action requires or not the presence of additional couplings of the type of Eqs. (4) and (5), as counterterms to absorb dimensional regularization poles $\propto (D-4)^{-1}$ (such poles are indeed linked to the possible ambiguities expected to arise at 5PN in the point-mass dynamics; see the discussion in Sec. 5 of [18]; see also Sec. 7 of [26]). We leave to future work a clarification of this subtle issue.

[3]More precisely, Eq. (4) describes only the effects that are *linear* in tidal deformations (and which preserve *parity*). If one wished to also consider *nonlinear* tidal effects one should augment the *quadratic-only* terms (5) by higher-order nonminimal worldline couplings which are cubic, quartic, etc. … in $C_{\mu\alpha\nu\beta}$ and its gradients. The coefficients of such terms would then parametrize some nonlinear tidal effects, which have not been considered in the linear treatments of Refs. [13,14].

B. Leading-order (LO) tidal effects in the two body interaction Lagrangian

Let us first consider the *dynamical* effects, implied by (4) i.e. the tidal contribution to the Fokker Lagrangian describing the dynamics of two compact bodies after having integrated out the gravitational field, say

$$L(\boldsymbol{q}^A, \boldsymbol{v}^A) = L^{\rm point\ mass} + L^{\rm tidal}. \quad (6)$$

Here, $L^{\rm point\ mass}(q, v)$ denotes the (time-symmetric) interaction Lagrangian following from the point-mass action (2) (say after a suitable redefinition of position variables to eliminate higher derivatives). It is currently known at the 3PN level. The supplementary term $L^{\rm tidal}$ in Eq. (6) is of the symbolic form (keeping only powers of G and $1/c_0$)

$$L^{\rm tidal} \sim G^2\mu_2\Big(1 + \frac{1}{c_0^2} + G + \cdots\Big) + \frac{G^2\sigma_2}{c_0^2}\Big(1 + \frac{1}{c_0^2} + G + \cdots\Big) + G^2\mu_3\Big(1 + \frac{1}{c_0^2} + G + \cdots\Big) + \cdots. \quad (7)$$

Let us start by discussing the *leading-order* contributions associated with each tidal coefficient μ_ℓ or σ_ℓ. The leading term in the contribution linked to μ_ℓ is simply obtained from (4) by inserting the leading-order value of G_L^A, i.e. ($L \equiv a_1 \cdots a_\ell$)

$$G_L^A = [\partial_L U^{\rm ext}(\mathbf{x})]^A = \partial_L^A\Big(\frac{GM^B}{|z_A - z_B|}\Big), \quad (8)$$

where $B \neq A$ denotes the companion of body A in the considered binary system (A, $B = 1$, 2), and $|z_A - z_B|$ the distance between the two bodies. In addition, $\partial_L^A \equiv \partial^A_{a_1\cdots a_\ell}$, with $\partial_a^A \equiv \partial/\partial z_A^a$, denotes the differentiation with respect to z_A that appear after taking the limit where the field point $\boldsymbol{x}$ tends to z_A on the worldline of body A. Using

$$\partial_L^A \frac{1}{r_{AB}} = (-)^\ell (2\ell-1)!! \frac{\hat{n}^L_{AB}}{r_{AB}^{\ell+1}}, \quad (9)$$

where $n^a_{AB} \equiv (z_A^a - z_B^a)/r_{AB}$, $r_{AB} \equiv |z_A - z_B|$, and where the hat denotes a symmetric trace-free (STF) projection, and the fact that [see, e.g., Eq. (A25) of [27]]

$$\hat{n}^L_{AB}\hat{n}^L_{AB} = \hat{n}^L_{AB}n^L_{AB} = \frac{\ell!}{(2\ell-1)!!}, \quad (10)$$

one easily finds that the leading Lagrangian contribution proportional to μ_ℓ reads

$$L_{\mu_\ell^A} = \frac{(2\ell-1)!!}{2}\mu_\ell^A \frac{(GM^B)^2}{r_{AB}^{2\ell+2}} = k_\ell^A G (M^B)^2 \frac{R_A^{2\ell+1}}{r_{AB}^{2\ell+2}}. \quad (11)$$

Here we have used (1) to replace $G\mu_\ell^A$ in terms of the dimensionless Love number k_ℓ^A, and of the areal radius R_A of the NS. Note that, in a BNS system, one has to add two

different contributions: $L_{\mu_\ell^A} + L_{\mu_\ell^B}$. By contrast, in a BHNS system one has only $L_{\mu_\ell^A}$ if A denotes the NS.

Let us also evaluate the leading magnetic-type contribution, i.e. the term $\propto \sigma_2$ in (6). It is obtained by inserting in (4) the Newtonian-level value of the gravito-magnetic quadrupolar field $H_{ab}^{B/A}$ exerted by body B on body A. This is given by Eq. (6.27a) of [28], namely,

$$H_{ab}^{B/A} = -2G\partial_{ac}^A\left(\frac{\epsilon_{bcd}M^B v_{BA}^d}{r_{AB}}\right) - 2G\partial_{bc}^A\left(\frac{\epsilon_{acd}M^B v_{BA}^d}{r_{AB}}\right), \tag{12}$$

where $v_{BA}^d \equiv v_B^d - v_A^d$ is the relative velocity between B and A. A straightforward calculation then yields

$$L_{\sigma_2^A} = 12\sigma_2^A \frac{(GM^B)^2}{r_{AB}^6}\left[\left(\frac{\boldsymbol{v}_{AB}}{c_0}\right)^2 - \left(\frac{\boldsymbol{n}_{AB}\cdot\boldsymbol{v}_{AB}}{c_0}\right)^2\right]. \tag{13}$$

Note that the leading quadrupolar gravito-magnetic contribution (13) is smaller than the corresponding quadrupolar gravito-electric contribution

$$L_{\mu_2^A} = \frac{3}{2}\mu_2^A \frac{(GM^B)^2}{r_{AB}^6} \tag{14}$$

by a factor

$$8\frac{\sigma_2^A}{\mu_2^A}\left[\left(\frac{\boldsymbol{v}_{AB}}{c_0}\right)^2 - \left(\frac{\boldsymbol{n}_{AB}\cdot\boldsymbol{v}_{AB}}{c_0}\right)^2\right]. \tag{15}$$

In terms of the corresponding dimensionless Love numbers j_2 (defined in [13]) and k_2, the prefactor $8\sigma_2^A/\mu_2^A$ is equal to the dimensionless ratio $j_2/(4k_2)$. However, it was found in [13,14] that the magnetic Love number j_2 was much smaller than k_2. Typically, for a $\gamma = 2$ μ-polytrope and a compactness $c^A \sim 0.15$, one has $j_2 \simeq -0.02$, while $k_2 \sim 0.1$, so that $8\sigma_2/\mu_2 = j_2/(4k_2) \simeq -0.05$. In other words, the leading gravito-magnetic interaction (13) is equivalent (say for circular orbits) to a 1PN fractional correction factor, $1 + \alpha(v_{AB}/c_0)^2$, modifying the leading gravito-electric contribution (14), with $\alpha = 8\sigma_2/\mu_2 = j_2/(4k_2) \sim -0.05$. As we shall discuss below, the 1PN correction to (14), implied by (4), involves coefficients $\alpha^{1\mathrm{PN}}$ of order unity. We will therefore, in the following, neglect the contribution (13) which represents only a small fractional modification to the 1PN correction to (14). On the other hand, we shall retain some of the higher-degree gravito-electric contributions. Indeed, though, for instance, $L_{\mu_3^A} \propto 1/r_{AB}^8$ formally corresponds to a 2PN correction to $L_{\mu_2^A} \propto 1/r_{AB}^6$, its coefficient is much larger than that corresponding to an order-unity 2PN correction to Eq. (14) (see Table I).

Summarizing: the leading-order tidal contributions to the two body interaction Lagrangian are [from Eq. (11)]

$$L^{\mathrm{tidal}} = +G\sum_{\ell\geq 2}\left\{k_\ell^A (M^B)^2 \frac{R_A^{2\ell+1}}{r_{AB}^{2\ell+2}} + k_\ell^B (M^A)^2 \frac{R_B^{2\ell+1}}{r_{AB}^{2\ell+2}}\right\}, \tag{16}$$

where k_ℓ^A denotes the ℓth dimensionless Love number of a NS [11,13,14]. Note that the plus sign in Eq. (16) expresses the fact that the tidal interactions are *attractive*.

C. Structure of subleading (post-Newtonian) dynamical tidal effects

Leaving to future work [29] a detailed computation of higher-order relativistic tidal effects, let us indicate their general structure. Here, we shall neglect the effects which are nonlinear in the worldline couplings μ_ℓ^A of Eq. (4) (e.g. effects $\propto \mu_2^A \mu_2^A$) for two reasons. On the one hand, such effects are numerically quite small, even for close neutron stars (as we shall check below). On the other hand, a fully consistent discussion of such effects requires that one considers a more general version of nonminimal worldline couplings, involving terms which are cubic (or more nonlinear) in the curvature tensor and its covariant derivatives. Indeed, it is easily seen that a nonminimal coupling which is *cubic* in $G_{ab} \sim \mathcal{E}_{\alpha\beta}$ contributes to the dynamics at the same level that a 1PN correction to the coupling quadratic in G_{abc}.

In the quadratic-in-curvature approximation of Eq. (4), the part of the tidal interaction which is proportional to μ_ℓ^A will have the symbolic structure

$$S_{\mu^A} \sim \mu^A (GM^B)^2[1 + GM^A + GM^B + (GM^A + GM^B)^2 + \cdots], \tag{17}$$

where we indicate only the dependence on GM^A and GM^B, leaving out all the coefficients (symbolically replaced by 1), which depend on positions and velocities. The presence of an overall factor $(GM^B)^2$ comes from the fact that $G_\ell^A(z^\mu)$ in Eq. (4) (which denotes the *regularized* value of some gradient of the curvature tensor as the field point x tends to $z_A^\mu(s_A)$ on the worldline of M^A) is proportional to GM^B, so that it is vanishing when $M^B \to 0$, i.e. in the limit of a one body system. [We are considering here a two body system; in the more general case of an N body system we would have $G^A(z_A) \propto \sum_{B\neq A} GM^B$.] In a diagrammatic language (see e.g. [22]) the higher-order terms on the right-hand side (rhs) of Eq. (17) correspond to diagrams where, besides having the basic (quadratic in $h_{\mu\nu}$) vertex μ_A on the A worldline being connected by two gravity propagators to two GM_B sources on the B worldline, we also have some further gravity propagators connecting one of the worldlines either to one of the worldline vertices, or to some intermediate field vertex. Note that the information about the 1PN corrections to both gravito-electric (μ_ℓ) and gravito-magnetic (σ_ℓ) multipolar interactions (of any degree ℓ) is contained in the work of Damour, Soffel, and Xu [28,30,31]. We shall discuss below the effect of the subleading (post-Newtonian) terms in (17) on the EOB description of the dynamics of tidally interacting binary systems.

III. INCORPORATING DYNAMICAL TIDAL EFFECTS IN THE EFFECTIVE ONE BODY FORMALISM

A. General proposal

The EOB formalism [32–34] replaces the two body interaction Lagrangian (or Hamiltonian) by a Hamiltonian, of a specific form, which depends only on the relative position and momentum of the binary system, say $(\boldsymbol{q}, \boldsymbol{p})$. For a nonspinning BBH system, it has been shown that its dynamics, up to the 3PN level, can be described by the following EOB Hamiltonian (in polar coordinates, within the plane of the motion):

$$H_{\rm EOB}(r, p_{r_*}, p_\varphi) = Mc_0^2\sqrt{1 + 2\nu(\hat{H}_{\rm eff} - 1)}, \tag{18}$$

where

$$\hat{H}_{\rm eff} = \sqrt{p_{r_*}^2 + A(r)\left(1 + \frac{p_\varphi^2}{r^2} + z_3\frac{p_{r_*}^4}{r^2}\right)}. \tag{19}$$

Here $M = M_A + M_B$ is the total mass, $\nu \equiv M_A M_B/(M_A + M_B)^2$ is the symmetric mass ratio, and $z_3 \equiv 2\nu(4 - 3\nu)$. In addition we are using rescaled dimensionless (effective) variables, notably $r = r_{AB}c_0^2/GM$ and $p_\varphi = P_\varphi c_0/(GM_A M_B)$, and p_{r_*} is canonically conjugated to a tortoise modification of r [35].

A remarkable feature of the EOB formalism is that the complicated, original 3PN Hamiltonian (which contains many corrections to the basic Newtonian Hamiltonian $\frac{1}{2}\boldsymbol{p}^2 - 1/r$) can be replaced by the simple structure (18) and (19) whose two crucial ingredients are (i) a double square-root structure $H_{\rm EOB} \sim \sqrt{1 + \sqrt{\boldsymbol{p}^2 + \cdots}}$, and (ii) the condensation of most of the nonlinear relativistic gravitational interactions in one function of the (EOB) radial variable: the basic radial potential $A(r)$. In addition, the structure of the function $A(r)$ is quite simple. At the 3PN level it is simply equal to

$$A^{\rm 3PN}(r) = 1 - 2u + 2\nu u^3 + a_4\nu u^4, \tag{20}$$

where $a_4 = 94/3 - (41/32)\pi^2$, and $u \equiv 1/r = GM/(c_0^2 r_{AB})$. It was recently found [1] that an excellent description of the dynamics of BBH systems is obtained by (i) augmenting the presently computed terms in the PN expansion (20) by additional 4PN and 5PN terms, and by (ii) Padé resumming the corresponding 5PN Taylor expansion of the A function. In other words, BBH (or point-mass) dynamics is well described by a function of the form

$$A^0(r) = P_5^1[1 - 2u + 2\nu u^3 + a_4\nu u^4 + a_5\nu u^5 + a_6\nu u^6], \tag{21}$$

where P_m^n denotes an (n, m) Padé approximant. It was found in Ref. [1] that a good agreement between EOB and numerical relativity binary black-hole waveforms is obtained in an extended bananalike region in the (a_5, a_6) plane approximately extending between the points $(a_5, a_6) = (0, -20)$ and $(a_5, a_6) = (-36, +520)$. In this work we shall select the values $a_5 = -6.37$, $a_6 = +50$ which lie within this good region.

Our proposal for incorporating dynamical tidal effects in the EOB formalism consists of preserving the simple general structure (18) and (19) of the EOB Hamiltonian, but to modify the BBH radial potential (21) [which corresponds to the point-mass action (2)] by augmenting it by some tidal contribution. In other words the proposal is to use Eqs. (18) and (19) with

$$A(r) = A^0(r) + A^{\rm tidal}(r). \tag{22}$$

B. Incorporating LO dynamical tidal interactions

Let us show that, at the LO, one can use a tidal contribution of the form

$$A_{\rm LO}^{\rm tidal}(r) = -\sum_{\ell\geq 2}\kappa_\ell^T u^{2\ell+2}, \tag{23}$$

with some dimensionless coefficient κ_ℓ^T.

Indeed, if we keep only the Newtonian approximation of the full EOB Hamiltonian (18) and (19) [using $A(r) \equiv 1 + \bar{A}(r)$ with $\bar{A}(r) = -2GM/(c_0^2 r_{AB}) + \cdots$ being 1PN small as $1/c_0^2 \to 0$] one finds (with $\mu \equiv M_A M_B/M$ the reduced mass of the system)

$$H_{\rm EOB} \simeq Mc_0^2 + \frac{1}{2}\mu\boldsymbol{p}^2 + \frac{1}{2}\mu\bar{A}(r) + \mathcal{O}\left(\frac{1}{c_0^2}\right), \tag{24}$$

which exhibits the role of $\frac{1}{2}\mu\bar{A}(r)$ as being the interaction energy. Decomposing $\bar{A}(r) = \bar{A}^0(r) + A^{\rm tidal}(r)$, and remembering that there is a sign reversal between the interaction energy and the interaction Lagrangian, we see that the terms (16) can be converted in a contribution to the $A(r)$ potential of the form (23), if the coefficients κ_ℓ^T take the values

$$\begin{aligned}\kappa_\ell^T &= 2k_\ell^A\frac{M_B}{M_A}\left(\frac{R_A c_0^2}{G(M_A + M_B)}\right)^{2\ell+1} + 2k_\ell^B\frac{M_A}{M_B}\\ &\quad\times\left(\frac{R_B c_0^2}{G(M_A + M_B)}\right)^{2\ell+1}\\ &= 2\frac{M_B M_A^{2\ell}}{(M_A + M_B)^{2\ell+1}}\frac{k_\ell^A}{c_A^{2\ell+1}} + 2\frac{M_A M_B^{2\ell}}{(M_A + M_B)^{2\ell+1}}\frac{k_\ell^B}{c_B^{2\ell+1}}.\end{aligned} \tag{25}$$

In the second form, we have introduced the compactness parameters of the stars: $c_A \equiv GM_A/(R_A c_0^2)$. It is interesting to note that the dimensionless tidal parameters that enter the EOB dynamics are (when $M_A \sim M_B$) the ratios $k_\ell^A/c_A^{2\ell+1}$, rather than the Love numbers k_ℓ^A. Let us also note that the velocity of light c_0 formally appears in the numerator of κ_ℓ^T. This is related to the fact that, contrary to the coefficients of the successive powers of u that enter the BBH EOB potential $A^0(r)$ which are (roughly speaking)

pure numbers of order unity, the coefficients κ_ℓ^T entering the tidal contribution $A^{\rm tidal}(r)$ will tend to be much larger than unity (and to increase with ℓ). For instance, we shall typically find that $\kappa_2^T = \mathcal{O}(100)$. This numerical difference makes it consistent to add to $A^0(r)$ (which is known for sure only up to u^4 terms, i.e. the 3PN level) additional terms $\propto u^6 + u^8 + \cdots$ that would formally correspond to 5PN + 7PN + $\cdots$ contributions if their coefficients were of order unity (at least in the parametric sense).

Finally, to illustrate the typical numerical values of the EOB tidal parameters we give in Table I the values of κ_2^T for five paradigmatic systems, one equal-mass BNS, and four BHNS systems of mass ratios $q \equiv M_{\rm BH}/M_{\rm NS}$ taking the values $q = (1, 2, 4, 10)$. For simplicity the neutron-star EOS is taken to be a polytrope $p = K\rho^\Gamma$ with $\Gamma = 2$ (here ρ denotes the rest-mass density). As Table I is plotting dimensionless quantities, the value of the polytropic constant K is not important, only the compactness of the NS matters: we have taken it to be $c_A = 0.15$. This value, for instance, corresponds to a NS of mass $1.35M_\odot$ and radius 13.3 km. Note that the main dependence on the EOS in κ_ℓ^T (say for the equal-mass BNS case) comes from $\kappa_\ell^T \propto (1/c_A)^{2\ell+1}$. Therefore, if one were considering a NS of different compactness, κ_2^T would be approximately given by $\kappa_2^T \sim 116(0.15/c_A)^5$.

One sees in Table I that the dimensionless tidal parameter κ_2^T is a strongly decreasing function of the mass ratio. This is analytically understood by looking at Eq. (25). When the label B refers to a black hole (so that $k_\ell^B = 0$), denoting $q \equiv M_{\rm BH}/M_{\rm NS} = M_B/M_A$, we have $\kappa_\ell^T = \kappa_\ell^A$ where

$$\kappa_\ell^A = 2\frac{k_\ell^A}{c_A^{2\ell+1}}\frac{q}{(1+q)^{2\ell+1}}. \tag{26}$$

Here c_A denotes as above the compactness of the NS. Therefore, as soon as the mass ratio q is significantly larger than 1, we see that κ_ℓ^A contains a small factor $q^{-2\ell}$ that suppresses the tidal contribution. As a consequence, GW-observable tidal effects will be strongly suppressed in realistic BHNS systems. Note, however, that it might be quite useful to compare numerical relativity simulations of artificial BHNS systems of mass ratio $q \sim 1$ to their EOB description to probe the analytical understanding of the late inspiral and plunge phase. In particular, we note that, as a function of q, $\kappa_2^T \propto q/(1+q)^5$ vanishes both when $q \to 0$ and $q \to \infty$ and reaches a maximum value when $q = M_{\rm BH}/M_{\rm NS} = 1/4$. Moreover the maximum value of κ_2^T is larger than the value of κ_2^T for a corresponding *equal-mass* BNS system by a factor $4^6/5^5 = 1.311$. We suggest that the numerical study of such astrophysically irrelevant BHNS systems (with $M_{\rm BH}/M_{\rm NS} \sim 1/4$) can be quite useful for improving our understanding of tidal interactions in strongly interacting (near contact) regimes.

C. Parametrizing higher-order dynamical tidal corrections

Above we discussed the LO contribution of tidal interactions to the EOB radial potential $A(r)$. We also discussed the structure of subleading (post-Newtonian) contributions to tidal interactions, Eq. (17). Comparing the structure (17) to the part of the EOB action linear in $A^{\rm tidal}$, which is proportional to the product of $A^{\rm tidal}$ by the reduced mass $\mu = M_A M_B/(M_A + M_B)$, we see that the general structure of the tidal contributions to the $A(r)$ potential is

$$A^{\rm tidal}_{\mu_A} \sim \frac{M_A + M_B}{M_A M_B}\mu^A \frac{(GM_B)^2}{r^{\ell+2}}\left[1 + \frac{GM_A}{r} + \frac{GM_B}{r} + \left(\frac{GM_A}{r} + \frac{GM_B}{r}\right)^2 + \cdots\right], \tag{27}$$

where we invoked dimensional analysis to insert appropriate powers of the (EOB) radial separation r. [Contrary to the action (17) which also depends on velocities (and higher-derivatives), the EOB radial potential depends only on the radius r.]

In other words, if we separate, for each multipolar order, the μ_A and μ_B contributions to $A^{\rm tidal}$,

$$A^{\rm tidal} = \sum_{\ell\geq 2} A^{\mu_\ell^A} + \sum_{\ell\geq 2} A^{\mu_\ell^B}, \tag{28}$$

we can write

$$A^{\mu_\ell^A} = A^{\mu_\ell^A}_{\rm LO}[1 + \alpha_1^{A(\ell)}u + \alpha_2^{A(\ell)}u^2 + \alpha_3^{A(\ell)}u^3\cdots], \tag{29}$$

where

$$A^{\mu_\ell^A}_{\rm LO} \equiv -\kappa_\ell^A u^{2\ell+2} \tag{30}$$

is the part of $A^{\rm tidal}_{\rm LO}$, Eq. (23), which is linear in μ_ℓ^A, or k_ℓ^A, i.e.

$$\kappa_\ell^A = 2k_\ell^A \frac{M_B}{M_A}\left(\frac{R_A c_0^2}{G(M_A + M_B)}\right)^{2\ell+1}. \tag{31}$$

Similarly, one will have

$$A^{\mu_\ell^B} = A^{\mu_\ell^B}_{\rm LO}[1 + \alpha_1^{B(\ell)}u + \alpha_2^{B(\ell)}u^2 + \alpha_2^{B(\ell)}u^3 + \cdots]. \tag{32}$$

The coefficient $\alpha_1^{A(\ell)}$ represents the next-to-leading order (NLO) fractional correction to the leading-order $A^{\mu_\ell^A}_{\rm LO}$ (i.e. a 1PN fractional correction), while $\alpha_2^{A(\ell)}$ represents the next-to-next-to-leading-order (NNLO) correction (i.e. a 2PN fractional correction), etc. These coefficients are not pure numbers, but rather function of the two dimensionless mass ratios

$$X_A \equiv \frac{M_A}{M_A + M_B}, \tag{33}$$

$$X_B \equiv \frac{M_B}{M_A + M_B} \equiv 1 - X_A. \tag{34}$$

The coefficients entering Eq. (32) are obtained from those entering (29) by the interchange of X_A and X_B, i.e. $\alpha_n^{A(\ell)}(X_A, X_B) = \alpha_n^{B(\ell)}(X_B, X_A)$. The symbolic structure (27) would naively suggest that $\alpha_1^{A(\ell)}$ is a linear combination of X_A and X_B and that $\alpha_2^{A(\ell)}$ is a combination of X_A^2, $X_A X_B$, and X_B^2. However, as the reformulation of (17) in terms of an EOB potential (27) involves a contact transformation that depends on the symmetric mass ratio $\nu \equiv X_A X_B$ (see Ref. [32]), the mass-ratio dependence of $\alpha_n^{A(\ell)}$ might be more complicated. Note that, by using the identity $X_A + X_B \equiv 1$, one can, e.g., express $\alpha_n^{A(\ell)}$ in terms of X_A only. (Then $\alpha_n^{B(\ell)}$ will be the same function of X_B as $\alpha_n^{A(\ell)}$ of X_A.) Note also that, if one wishes, one can, for each value of ℓ factorize the total LO terms $-\kappa_\ell^T u^{2\ell+2}$, and write

$$A^{\rm tidal} = \sum_{\ell \geq 2} - \kappa_\ell^T u^{2\ell+2} \hat{A}_\ell^{\rm tidal}, \tag{35}$$

where

$$\hat{A}_\ell^{\rm tidal} \equiv 1 + \bar{\alpha}_1^{(\ell)} u + \bar{\alpha}_2^{(\ell)} u^2 + \cdots, \tag{36}$$

with

$$\bar{\alpha}_n^{(\ell)} \equiv \frac{\kappa_\ell^A \alpha_n^{A(\ell)} + \kappa_\ell^B \alpha_n^{B(\ell)}}{\kappa_\ell^A + \kappa_\ell^B}. \tag{37}$$

Using Eqs. (4.27) and (4.29) of [30], or Eq. (3.33) of [31], together with effective-action techniques, a recent calculation [29] gave the following result for the 1PN coefficient of multipolar order $\ell = 2$, $\alpha_1^{A(2)}$, namely,

$$\alpha_1^{A(2)} = \tfrac{5}{2} X_A. \tag{38}$$

More work is needed to determine the higher-degree and/or higher-order coefficients $\alpha_n^{A(\ell)}(X_A, X_B)$, and thereby the coefficients $\bar{\alpha}_n^{(\ell)}$ entering Eq. (37). Below, we shall focus on the equal-mass case where the coefficients $\alpha_n^{A(\ell)}$ become pure numbers.

Here we shall explore several possible proposals for including higher-order PN corrections in tidal effects. The first proposal consists of truncating Eq. (36) at 1PN order in a straightforward Taylor way, i.e. to consider a PN correcting factor to the EOB radial potential of the form

$$\hat{A}_\ell^{\rm tidal} = 1 + \bar{\alpha}_1^{(\ell)} u. \tag{39}$$

The second proposal consists of considering a PN correcting factor which has a Padé-resummed structure, i.e.

$$\hat{A}_\ell^{\rm tidal} = (1 - \bar{\alpha}_1^{(\ell)} u)^{-1}. \tag{40}$$

Our third proposal consists of considering a PN correcting factor which would result from having a shift between the EOB radial coordinate and the radial coordinate appearing most naturally in a Newtonian-like tidal interaction ($\propto 1/r^{2\ell+2}$),

$$\hat{A}_\ell^{\rm tidal} = (1 - \tilde{\alpha}_1^{(\ell)} u)^{-(2\ell+2)}. \tag{41}$$

We use here a different notation for the 1PN coefficient, $\tilde{\alpha}_1^{(\ell)}$, as a reminder that, for instance, when $\ell = 2$, the parametrization (41) corresponds to a 1PN coefficient in the parametrization (39) given by

$$\bar{\alpha}_1^{(2)} = 6 \tilde{\alpha}_1^{(2)}. \tag{42}$$

Finally, we shall also consider an additional, fourth, proposal consisting of taking a PN correction function of the form

$$\hat{A}_\ell^{\rm tidal} = 1 + \bar{\alpha}_1^{(\ell)} u + \bar{\alpha}_2^{(\ell)} u^2, \tag{43}$$

where $\bar{\alpha}_1^{(\ell)}$ is analytically computed by means of Eqs. (37) and (38); i.e., $\bar{\alpha}_1^{(\ell)} = 1.25$ in the equal-mass case.

IV. COMPARING EOB TO NUMERICAL RELATIVITY RESULTS IN WAVELESS CIRCULAR BINARIES

The aim of this section is to compare stationary quasicircular configurations of neutron-star binaries computed, on the one hand, in the analytical framework outlined above and, on the other hand, in the numerical framework recently implemented by Uryū *et al.* [15] (see also [16]). The quantity from both frameworks that we shall compare is the binding energy E_b as a function of the orbital frequency Ω. (In the following, we generally set c_0 to 1, except when it is useful to indicate the PN order.)

A. Tidally interacting BNS circular configurations in the EOB framework

1. BNS binding energy in the EOB framework

As an application of the formalism discussed so far, we consider in this section binaries in exactly circular orbits, in absence of radiative effects (these will be discussed in the following section).

As the EOB formalism is based on a Hamiltonian description of the conservative dynamics, the stable circular orbits correspond to minima, with respect to r, of the radial potential $H_{\rm EOB}^{\rm radial}(r, p_\varphi) \equiv H_{\rm EOB}(r, p_{r_*} = 0, p_\varphi)$. Minimizing $H_{\rm EOB}^{\rm radial}(r, p_\varphi)$ is equivalent to minimizing the corresponding effective Hamiltonian $\hat{H}_{\rm eff}$, or, its square, i.e.

$$(\hat{H}_{\rm eff}^{\rm radial})^2(r, p_\varphi) = A(r)\left(1 + \frac{p_\varphi^2}{r^2}\right) \equiv A(u) + p_\varphi^2 B(u). \tag{44}$$

Here, we have used the shorthand notation $u \equiv 1/r = GM/R$ and $B(u) \equiv u^2 A(u)$. Minimizing (44) with respect to r (or, equivalently, u), for a given (scaled) total angular momentum $p_\varphi \equiv J^{\rm tot}/GM\mu$, yields the following equation:

$$A'(u) + p_\varphi^2 B'(u) = 0, \tag{45}$$

where the prime denotes a u derivative. This leads to the following parametric representation of the squared angular momentum:

$$j^2(u) = -\frac{A'(u)}{(u^2 A(u))'} \quad \text{(circular orbits)}, \tag{46}$$

where we use the letter j to denote the value of p_φ along the sequence of circular orbits. Inserting this u-parametric representation of j^2 in Eq. (19) defines the u-parametric representation of the effective Hamiltonian $\hat{H}_{\rm eff}(u)$. We can then obtain (at least numerically) $\hat{H}_{\rm eff}$ as a function of Ω by eliminating u between $\hat{H}_{\rm eff}(u)$ and the corresponding u-parametric representation of the frequency obtained by the angular Hamilton equation of motion in the circular case

$$GM\Omega(u) = \frac{1}{\mu}\frac{\partial H_{\rm EOB}}{\partial j} = \frac{MA(u)j(u)u^2}{H_{\rm EOB}\hat{H}_{\rm eff}}, \tag{47}$$

where $H_{\rm real}$ denotes the real EOB Hamiltonian

$$H_{\rm EOB} = M\sqrt{1 + 2\nu(\hat{H}_{\rm eff} - 1)}. \tag{48}$$

In this situation, the binding energy E_b of the system is simply given by

$$E_b(\Omega) = H_{\rm EOB} - M = M\{\sqrt{1 + 2\nu(\hat{H}_{\rm eff} - 1)} - 1\}, \tag{49}$$

where M denotes, as above, the total mass $M = M_A + M_B$ of the system, and where one must eliminate u between Eqs. (47) and (49) to express the rhs in terms of Ω. Note that the function $E_b(\Omega)$ depends also on the choice of the following parameters: κ_ℓ^T, $\alpha_1^{A(\ell)}$, and $\alpha_1^{B(\ell)}$. Here we shall focus on the equal-mass case, and consider the dependence of $E_b(\Omega)$ only on $(\kappa_2^T, \kappa_3^T, \kappa_4^T)$ and restrict the parametrization of 1PN tidal effects to the consideration of a *single* 1PN tidal parameter $\bar{\alpha}_1$ that is taken to be the same for the three values of ℓ that we consider. In addition, we will incorporate 1PN corrections to tidal effects in the three aforementioned functional forms, Eqs. (39)–(41) and contrast their performances.

2. BNS binding energy in the PN framework

We also want to contrast the performance of the EOB approach (which represents a resummation of the dynamics of the binary system) with the standard nonresummed PN-based description of the binding energy of tidally interacting BNS, as used for instance in Ref. [36,37]. The PN-expanded binding energy is written in the form

$$E_b(\Omega) = E_{\rm point\ mass}(\Omega) + E^{\rm tidal}(\Omega), \tag{50}$$

where

$$E_{\rm point\ mass}(\Omega) = -\frac{\mu}{2}x\Big\{1 - \Big(\frac{3}{4} + \frac{1}{12}\nu\Big)x - \Big(\frac{27}{8} - \frac{19}{8}\nu + \frac{1}{24}\nu^2\Big)x^2 - \Big(\frac{675}{64} - \Big[\frac{34\,445}{576} - \frac{205}{96}\pi^2\Big]\nu + \frac{155}{96}\nu^2 + \frac{35}{5184}\nu^3\Big)x^3\Big\} \tag{51}$$

is the 3PN accurate post-Newtonian binding energy of two point masses as a function of the dimensionless orbital frequency parameter [19,38]

$$x = \Big(\frac{GM\Omega}{c_0^3}\Big)^{2/3}. \tag{52}$$

The expression of the tidal contribution $E^{\rm tidal}(\Omega)$ can be obtained for all values of the multipolar index ℓ by noting the following. Any (perturbative) power-law radial contribution to the interaction Hamiltonian of the form

$$\delta H(r) = -\frac{c_n}{r^n} \tag{53}$$

is easily shown to contribute a corresponding term

$$\delta E_b(\Omega) = +\Big(\frac{2}{3}n - 1\Big)\frac{c_n}{r_\Omega^n}, \tag{54}$$

where it should be noted that the sign of the tidal contribution flips between the Hamiltonian and the binding energy expressed as a function of the orbital frequency (r_Ω denoting the Newtonian value of r corresponding to a given circular orbit of frequency Ω). As a result, we have the leading-order contribution to the PN-tidal contribution

$$E_{\rm LO}^{\rm tidal}(\Omega) = +\frac{\mu}{2}\sum_{\ell\geq 2}\Big[\frac{2}{3}(2\ell + 2) - 1\Big]\kappa_\ell^T x^{2\ell+2}. \tag{55}$$

We shall also explore the effect of correcting $E_{\rm LO}^{\rm tidal}$ by a fractional 1PN contribution, i.e. to employ a PN-tidal contribution of the form

$$E^{\rm tidal}(x) = (1 + \bar{\alpha}_1' x)E_{\rm LO}^{\rm tidal}(x), \tag{56}$$

where the (approximate) link with the previously defined $\bar{\alpha}_1$ is

$$\bar{\alpha}_1' = \frac{11}{9}\bar{\alpha}_1. \tag{57}$$

Here the numerical coefficient $11/9$ arises as a consequence of the factor $2n/3 - 1$ in the result above (considered for $n = 6$ and $n = 7$).

B. BNS circular configurations in numerical relativity

1. Numerical framework of Uryū et al.

In a recent paper, Uryū *et al.* [15] constructed BNS systems in quasicircular orbits by solving numerically the full set of Einstein's equations. The important advance of this work with respect to previous analyses is the fact that Einstein equations are solved for all metric components, including the nonconformally flat part of the spatial metric. This goes beyond the common *conformally* flat approxi-

mation that is usually employed for the spatial geometry. The conformally flat approximation introduces systematic errors which enter the PN expansion already at the 2PN level (see the detailed calculation in Appendix B of Ref. [39]). Consistently with this analytical argument, it was found in Ref. [15] that the difference between conformally flat and nonconformally flat calculations is so large that it can mask the effect of tidal interactions for close systems. See, in this respect, the location of the conformally flat Isenberg-Wilson-Mathews (IWM) [40,41] binding energy curves in the two upper panels of Fig. 3 in Ref. [15]. Below we shall however emphasize that the *nonconformally* flat calculations of [15] *still* introduce significant systematic errors which enter the PN expansion *at the 3PN level*.

Since the new nonconformally flat results of Uryū *et al.* represent a definitive improvement with respect to previous calculations, it is appealing to see to what extent these new results agree with existing analytical descriptions. We extracted from Ref. [15] the six models which present the highest computational accuracy. These models were obtained by using EOS labeled 2H, HB, 2B, SLy, FPS, and BGN1H1. These labels refer to piecewise polytropic EOS. Note that in the cases of SLy, FPS, and BGN1H1 the corresponding piecewise polytropic EOS were proposed in Ref. [42] as approximations, above the nuclear density, to original tabulated EOS. On the other hand, Ref. [15] uses, below the nuclear density, a simplified *monopolytropic* EOS. In the cases of FPS and SLy, this implies that the tidal coefficients k_ℓ that we have computed for this work differ (by $\sim$20%) from the ones that we had previously computed in Ref. [13] that used the original tabulated EOS. For example, in the case of a neutron-star model described by the SLy EOS and having a compactness $c_A = 0.176$ (which corresponds to a mass of $M_A = 1.4M_\odot$), we obtain a dimensionless Love number $k_2^{(\mathrm{tab})} = 0.076\,99$ (which is consistent with the first line of Table I of Ref. [12]) if we use the tabulated EOS, while we obtain $k_2^{(\mathrm{ppoly})} = 0.091\,23$ if we use the piecewise polytropic EOS used in Ref. [15]. Note that the piecewise polytropic result is 18.5% larger than the tabulated one. Note, however, that the original paper [42] offered the possibility to use piecewise polytropic representations *both* for the (subnuclear) low-density EOS and for the higher density part. Using such more complete piecewise polytropic EOS representations then yields values of the k_2 Love number which are in good agreement with the ones computed from the original tabulated EOS [43].[4] We recommend in the future to use such more accurate piecewise polytropic representations that also cover the low-density EOS.

[4]It is also remarked by Lackey that even when using the simplified, high-density only, piecewise polytropic EOS the combined tidal coefficient $\mu_2 \sim k_2 R_A^5$ is more accurately represented than k_2 itself.

TABLE I. Comparing and contrasting tidal properties of BNS and BHNS systems. The NS model is obtained using a $\Gamma = 2$ polytropic EOS ($p = k\rho^\Gamma$) with compactness $c_A = 0.15$. We consider one (equal-mass) binary neutron-star system and several mixed black-hole–neutron-star binary systems with mass ratios $q = M_{\mathrm{BH}}/M_{\mathrm{NS}}$ varying between 1 and 10.

Model	q	κ_2^T	κ_3^T	κ_3^T
BNS	1	116.4635	373.791 8	1654.937 6
BHNS	1	58.2318	186.895 9	827.468 8
BHNS	2	15.3368	21.877 2	43.048 7
BHNS	4	2.3852	1.224 8	0.867 7
BHNS	10	0.1157	0.012 28	0.001 797

Among the six EOS that we retain, three, i.e. 2H, HB, and 2B, use two polytropic intervals, while the other three, i.e. SLy, FPS, and BGN1H1, use four polytropic intervals. We will thus have one dividing density,[5] denoted by ρ_0, for 2H, HB, and 2B, and three dividing densities, (ρ_0, ρ_1, ρ_2), for SLy, FPS, and BGN1H1. Here, ρ_0 indicates the dividing density between the lower density interval that approximates the subnuclear density part of the EOS (the crust) and the supernuclear density part. The values of (the base-ten logarithm of) ρ_0 (in g/cm^3) are displayed in the first column of Table I. For all EOS, the lower density interval (crust) is approximated by setting $(\Gamma_0, K_0) = (1.356\,92, 3.593\,89 \times 10^{13})$, where K_0 (here in cgs units) gives the pressure p in dyn/cm^2. The other dividing densities (for the four-parameter EOS) are fixed as $\rho_1 = 10^{14.7}$ g/cm^3 and $\rho_2 = 10^{15}$ g/cm^3. The corresponding adiabatic indices, $\{\Gamma_1, \Gamma_2, \Gamma_3\}$, taken from [15,42] are also given in Table I. For the implementation of the piecewise polytropic EOS we follow the procedure explained in Sec. III of [42] and in Sec. IID of [15].

For each selected EOS, we computed the sequence of equilibrium models with the related Love numbers k_ℓ up to $\ell = 4$. For the compactnesses corresponding to those used in [15] we display in Table II the k_ℓ^A's together with the values of mass and radius that we obtained from our calculation, to check consistency with the corresponding values of Table III of [15]. The small differences (at the 10^{-3}) level are probably due to the fact that we use the finite-digit value of the dividing density ρ_0 that they published.

2. Subtracting tidal effects from numerical relativity data

Let us start by noting two facts, that can be checked from the analytical expressions above, about the dependence of the binding energy on the tidal parameters κ_ℓ^T: (i) this dependence is to a very good approximation linear and (ii) the numerical effect of the κ_2^T strongly dominates over

[5]Here, following the notation of [42], we use the letter ρ to denote the rest-mass (baryon) density which was denoted by μ in our previous work [13].

TABLE II. Properties of NS models considered discussed in the numerical analysis of Ref. [15]. The EOS are represented as piecewise-polytropic functions (on four intervals) [42,44]. For the models considered, the present table is compatible with Table III of [15]. From left to right, the columns report the dividing density (in g cm^{-3}) between the low-density part (the crust) and the higher density part of the EOS; the four adiabatic indices for each polytropic interval, $\{\Gamma_0, \Gamma_1, \Gamma_2, \Gamma_3\}$; the compactness $c_A = GM_A/(c_0^2 R_A)$; the NS mass M_A (in $M_\odot$) and the NS radius R_A (in km); and the Love numbers k_2^A, k_3^A, and k_4^A.

Model	$\log(\rho_0)$	Γ_0	Γ_1	Γ_2	Γ_3	c	M_A	R_A	k_2^A	k_3^A	k_4^A
2H	13.847	1.356 92	3.0	3.0	3.0	0.130 97	1.3507	15.229	0.1342	0.0407	0.0168
HB	14.151	1.356 92	3.0	3.0	3.0	0.171 81	1.3507	11.608	0.0946	0.0260	0.0097
2B	14.334	1.356 92	3.0	3.0	3.0	0.205 00	1.3505	9.728	0.0686	0.0174	0.0059
SLy	14.165	1.356 92	3.005	2.988	2.851	0.173 85	1.3499	11.466	0.0928	0.0254	0.0095
FPS	14.220	1.356 92	2.985	2.863	2.600	0.186 31	1.3511	10.709	0.0805	0.0214	0.0077
BGN1H1	14.110	1.356 92	3.258	1.472	2.464	0.157 92	1.3490	12.614	0.1059	0.0307	0.0120

that of the higher degree κ_ℓ^T's. For example, if we take the tidal coefficients listed in Table I (which correspond to the SLy EOS, which yields a radius $\sim$11.5 km for $1.35M_\odot$, which is in the middle of the realistic range of NS radii), we find that the tidal contributions to the binding energy would reach, if they were extended to the maximum frequency that we shall explore here, namely, $GM\Omega_{\max} = 0.060$, the following values: the κ_2^T contribution to E_b/M is $\sim 3.6 \times 10^{-4}$, the κ_3^T contribution is smaller than the κ_2^T by a factor 0.053, and the κ_4^T is smaller than the κ_2^T one by a factor $\sim 3.85 \times 10^{-3}$.

These two facts allow us to approximately subtract tidal effects from NR data. Indeed, if we assume that the binding energy computed with a certain equation state $(\mathrm{EOS})_I$ is approximately given by

$$E_b(\Omega; I) \approx h_0(\Omega) + (\kappa_2^T)_I h_2(\Omega), \tag{58}$$

we can use the NR data for two different EOS, labeled by (I, J) to compute, separately

$$h_0(\Omega) \approx \frac{(\kappa_2^T)_I E_b(J) - (\kappa_2^T)_J E_b(I)}{(\kappa_2^T)_I - (\kappa_2^T)_J}, \tag{59}$$

$$h_2(\Omega) \approx \frac{E_b(I) - E_b(J)}{(\kappa_2^T)_I - (\kappa_2^T)_J}. \tag{60}$$

Most importantly we see that Eq. (59) allows us to compute from the binding energies of two BNS sequences a third binding energy function, h_0, which approximately represents the binding energy of *nontidally interacting* neutron stars, i.e. the binding energy curve of two point masses. The result of computing the rhs of Eq. (59) for five pairs (I, J) of EOS having sufficiently different κ_2^T's is displayed in the top-left panel of Fig. 1. Two important lessons can be drawn from this figure: (i) The subtraction procedure defined by Eq. (59) is remarkably able to define "tidal-free" energy curves that are essentially on top of each other; this confirms that our procedure succeeds in subtracting out the EOS dependence of the binding energy curves. (ii) However, the resulting universal h_0 curve still differs significantly both from the EOB point-mass curve (black solid lines) and the PN point-mass one (black dashed lines). This second issue will be addressed in the next section.

We shall not display here the result of computing the h_2 part of the binding energy curve, Eq. (60), because it is more sensitive than h_0 both to numerical noise (in the original NR data) and to the presence of higher-order tidal PN contributions. Below, we shall address the issue of determining the tidal contributions to E_b with a different approach.

3. Detecting and subtracting systematic errors in NR data

Here we address the issue (ii) mentioned in the previous section. Indeed, our subtraction procedure has given us access to the "universal," EOS-independent part of the energy curve h_0. However, we have seen that h_0 still significantly differs from the analytical point-mass models. We think that the origin of this discrepancy is the presence of remaining systematic errors in the current nonconformally flat approach to BNS systems. Though the nonconformally flat integration scheme of Uryū *et al.* is an improvement over previous work, it is however still only an approximation to the exact solution describing two BNS interacting in a (conservative) time-symmetric manner (half-retarded–half-advanced). Here we shall only use the data obtained by Ref. [15] called the waveless approximation. In their approach, waveless means setting to zero the time derivative of the conformal spatial metric (in a certain gauge): $\partial_t \tilde{\gamma}_{ab} = 0$. As the NR gauge is rather similar to the Arnowitt-Deser-Misner transverse-traceless (ADM-TT) gauge used in the 3PN calculation of the interaction Hamiltonian of a two point-mass system in Refs. [19,45], we can see, by looking at the analytical expression of the 3PN-accurate ADM Hamiltonian, that neglecting the terms containing $\pi_{ab}^{\mathrm{TT}} \sim \partial_t \tilde{\gamma}_{ab}$ means neglecting some of the terms that contribute at the 3PN level. [The simplest of these terms is the kinetic field energy term proportional to $\int d^3x (\pi_{ab}^{\mathrm{TT}})^2$.] This analytical argument suggests that the current NR data miss some 3PN contributions, i.e. they miss some terms proportional to x^4 in the binding energy curve. We are therefore entitled to assume that the discrep-

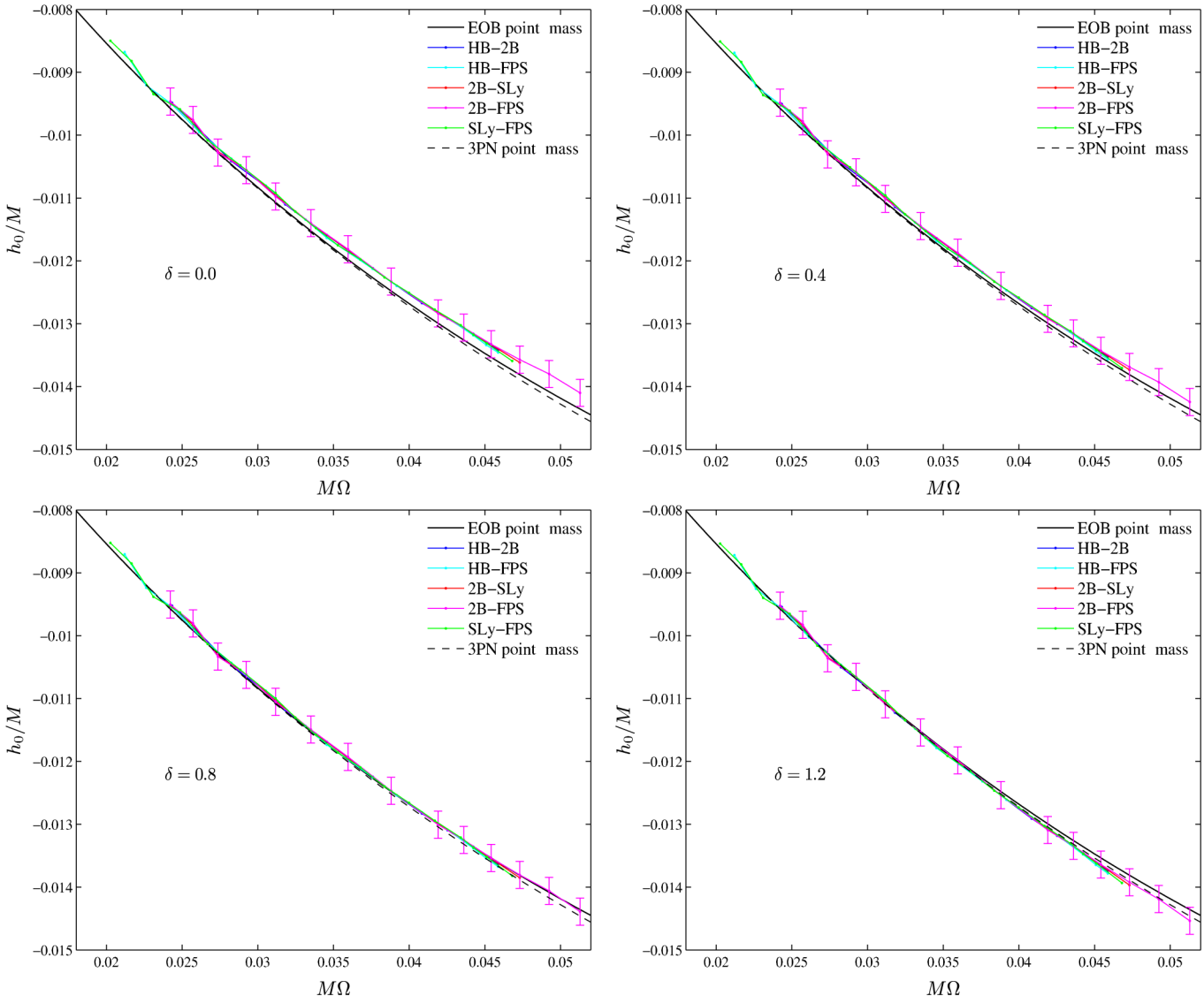

FIG. 1 (color online). Comparison between various δ-corrected h_0's [defined in Eq. (59)] and the EOB (resummed, solid lined) and 3PN (nonresummed, dashed lined) point-mass representations of the binding energy. The top-left panel illustrates (i) the universality of the tidally corrected energy curve $h_0(M\Omega)$ and (ii) the fact that it is in significant disagreement with all the analytical predictions, notably on the low-frequency side. The value $\delta = 0.8$ (lower-left panel) for the correction $\Delta E_b(\Omega) = \delta x^4$ lies at the center of the acceptable interval $0.4 \leq \delta \leq 1.2$ illustrated in the other panels.

ancy displayed in the top-left panel of Fig. 1 between the NR h_0 and the point-mass analytical curves is, to leading order, given by an expression of the type $\Delta E_b(\Omega) = \delta x^4$ with an EOS-independent numerical coefficient δ that we expect to be of order unity. Indeed, the lower-left panel of Fig. 1 exhibits the fact that, by subtracting $\Delta E_b(\Omega) = \delta x^4$, with $\delta = 0.8$ (see below) from all the individual h_0 curves, we can reach a good visual agreement with both analytical point-mass models. (Note that the approximate best-fit value of δ is mainly determined by the discrepancy numerical relativity/analytical relativity on the lower-frequency part of the panel, say for $M\Omega < 0.035$ where the contribution to tidal effects is relatively negligible.)

The remaining differences in this right panel are compatible with the known level of numerical errors in the NR data (see Fig. 4 of Ref. [15]). Indeed [15] has used the virial theorem to gauge some of the numerical errors in their calculation by comparing two measures of the total mass of the system (Komar and ADM). The resulting (absolute value) differences in binding energy, say $\delta^v E_b$, are in general at the level $10^{-4}M$. We used these differences to estimate formal error bars on the various energy curves that we use in this work. More precisely, in E_b energy curves we add (starting with Fig. 1) error bars of one-sided amplitude $\pm\frac{1}{2}\delta^v E_b$, so that the length of the two-sided error bars corresponds to the virial error. As Fig. 1 concerns

a quantity, h_0, defined as a linear combination of NR data [see Eq. (59)], we conservatively estimated error bars on the h_0 curve corresponding to the pair 2B-FPS by linearly combining in absolute values the corresponding individual errors. We use these error bars to gauge the quality of the other h_0 curves (which do not extend as far in the high frequency range). This conservative estimate of the total error seems appropriate to the present situation where the errors are not random, but rather systematic. (Note, however, that these error bars seem to be too conservative in the lower-frequency part of the panels because they exceed the distance between the h_0 curves and the point-mass models.) Using these error bars we can now roughly estimate a range of acceptable values of the NR correcting parameter δ. As illustrated in the four panels of Fig. 1, the range $0.4 \leq \delta \leq 1.2$ is such that the δ-corrected NR-deduced h_0 curves are within one formal sigma from both point-mass analytical models. We shall use this range below to estimate a corresponding range of probable values of the 1PN tidal parameter $\bar{\alpha}_1^{(2)}$.

4. Least-square analysis: constraining next-to-leading-order (1PN) tidal effects from numerical relativity data

In this section we shall firm up the previous analysis and make it more quantitative by using a least-square procedure. For each EOS, labeled by index I, we have 20 NR data points, Ref. [15], $E^{\mathrm{Ury\bar{u}}}$, where the index n_I varies from 1 to 20. We retain in our analysis six EOS; $I = (2\mathrm{H}, \mathrm{HB}, 2\mathrm{B}, \mathrm{FPS}, \mathrm{SLy}, \mathrm{BGN1H1})$. Let us then define the following formal χ^2 function, measuring the (squared) distance between NR and EOB:

$$\chi^2(\bar{\alpha}_1, \delta) = \sum_{I,n} \left[\left(\frac{E_b^{\mathrm{Ury\bar{u}}}(x_n; I)}{M} - \delta x_n^4 \right) - \frac{E_b^{\mathrm{EOB}}(x_n; \bar{\alpha}_1, I)}{M} \right]^2. \quad (61)$$

Here, x is the frequency parameter defined in Eq. (52) and the index n runs (for each EOS labeled I) over the sample of numerical data from 1 to 20, so that χ^2 contains 120 terms in all. We are interested in studying the dependence of χ^2 over the two variables $(\delta, \bar{\alpha}_1)$. Here δ denotes the coefficient of a 3PN subtraction to NR data of the type that we discussed in the previous section (as motivated by the neglect of some 3PN terms in the waveless approximation). As explained above, we shall restrict the variation of δ to the range $0.4 \leq \delta \leq 1.2$. For simplicity, we shall actually sample this interval through the three values $\delta = (0.4, 0.8, 1.2)$. On the other hand, the coefficient $\bar{\alpha}_1$ parametrizes a possible NLO 1PN correction to the tidal effects. We will use the three different descriptions of NLO tidal effects delineated in Eqs. (39)–(41).

We wish to use the least-square method, i.e., minimizing the EOB-NR "distance" function $\chi^2(\bar{\alpha}_1, \delta)$, to constrain the values of $(\bar{\alpha}_1, \delta)$. However, we find that $\chi^2(\bar{\alpha}_1, \delta)$ remains close (on the scale of the NR error bars) to its global minimum in a valley which extends over a significant region of the $(\bar{\alpha}_1, \delta)$ plane. This means that, given the present error level in numerical data, we cannot meaningfully and simultaneously select preferred values for $(\bar{\alpha}_1, \delta)$. As a substitute, we shall exhibit the sections of the χ^2 valley that correspond to the three values of δ selected visually in Fig. 1. In other words, we now fix δ (to one of its three values) in Eq. (61) and consider the dependence of χ^2 on $\bar{\alpha}_1$. The resulting one-dimensional plots are exhibited in Fig. 2.

Each panel of Fig. 2 corresponds to a different modelization of NLO tidal effects: Taylor [upper panel, Eq. (39)], Padé (middle panel), Eq. (40) and radial shift (lower panel), Eq. (41). [In the radial-shift case, one uses as the horizontal axis $\bar{\alpha}_1$ the quantity $\bar{\alpha}_1^{(2)}$ defined by Eq. (42).] In addition, each panel contains three curves corresponding to the three above-selected values of δ: $\delta = 0.4$ (dash-dotted line, rightmost curve), $\delta = 0.8$ (solid line, middle curve), and $\delta = 1.2$ (dashed line, leftmost curve).

Let us start by focusing on the (solid) curves corresponding to the central value of δ, $\delta = 0.8$. We see that the preferred values of $\bar{\alpha}_1$ that they select (minimum of the curves) are $\bar{\alpha}_1 \approx 7$ for the Taylor model, $\bar{\alpha}_1 \approx 3.5$ for the Padé model, and $\bar{\alpha}_1 \approx 4.5$ for the radial-shift model. This shows that higher-order PN terms (differently included in the different models) have a significant effect on the determination of $\bar{\alpha}_1$. Note also that when $\delta = 1.2$ all the models tend to favor a lower value: $\bar{\alpha}_1 \sim 1$. The value of χ^2 at $\bar{\alpha}_1 = 0$ and $\delta = 1.2$ is $\chi^2(0, 1.2) = 5.665 \times 10^{-7}$. This formally corresponds to an average (squared) error level on the individual NR-EOB energy differences summed in χ^2 equal to $\sqrt{\chi^2(0, 1.2)/120} = 0.687 \times 10^{-4}$. This level is comparable to the virial error on each individual NR data point $\delta^v E_b/M \sim 10^{-4}$. It is therefore reasonable to use this level to select a range of values of $\bar{\alpha}_1$. Combining this range with the range of values of δ's means that, at this stage, the range of values of $\bar{\alpha}_1$ that is compatible with the NR data is obtained by taking the level surface $\chi^2(\bar{\alpha}_1, \delta) = \chi^2(0, 1.2)$ as the admissible bottom of the valley in the $(\bar{\alpha}_1, \delta)$ plane. This leads to the following admissible ranges: $0 \lesssim \bar{\alpha}_1 \lesssim 15.7$ for the Taylor model; $0 \lesssim \bar{\alpha}_1 \lesssim 4.8$ for the Padé model; $0 \lesssim \bar{\alpha}_1 \lesssim 7.5$ for the radial-shift model. It is clear that at this stage the fact that (as we have argued above) the NR data are polluted by some systematic errors (notably linked to unaccounted 3PN effects) prevents us from giving very significant constraints on the value of $\bar{\alpha}_1$. Note, in particular, that the value $\bar{\alpha}_1 = 5/4 = 1.25$ which follows (in the equal-mass case) from Eq. (38) is compatible with the present NR data (if we allow $\delta = 1.2$). In this respect, it is interesting to note that if we consider a model of the form Eq. (43) introduced above as a fourth possibility

$$\hat{A}^{\mathrm{tidal}} = 1 + \bar{\alpha}_1 u + \bar{\alpha}_2 u^2, \quad (62)$$

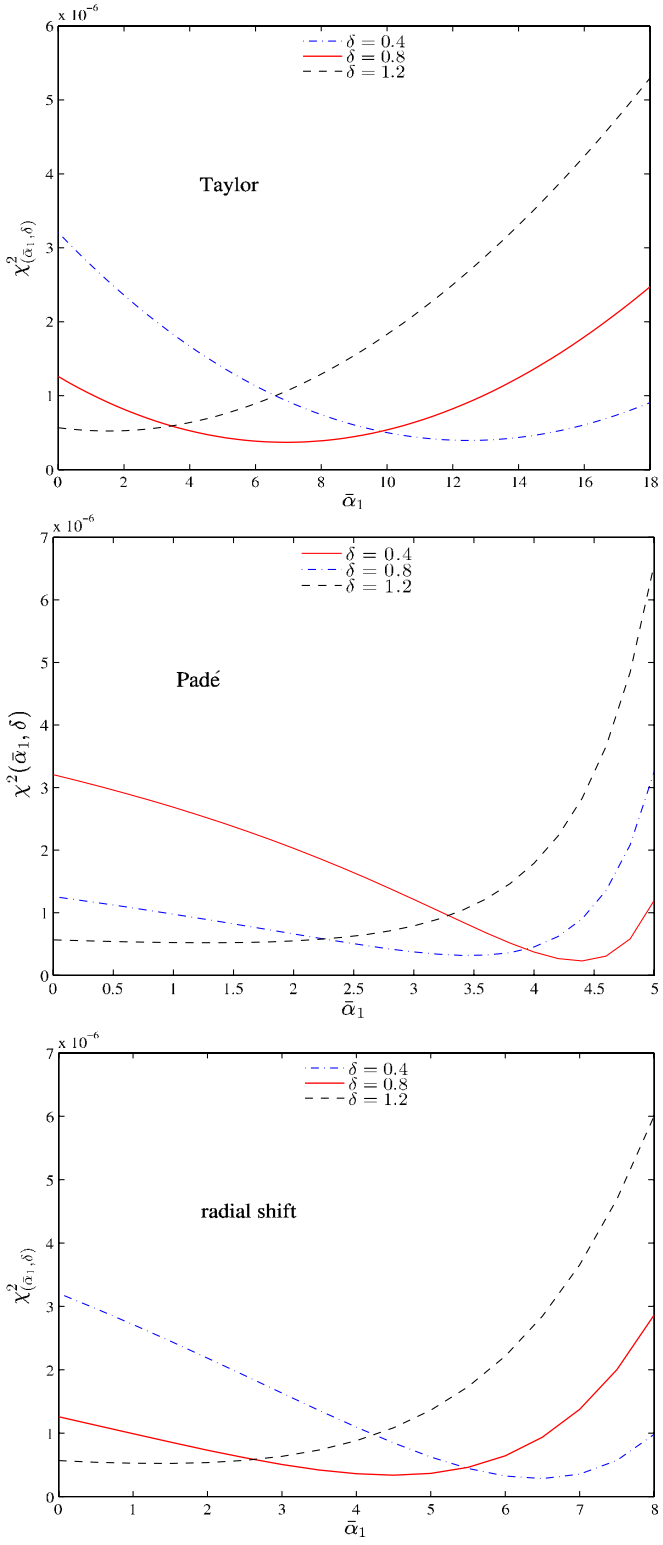

FIG. 2 (color online). Sections of the function $\chi^2(\bar{\alpha}_1, \delta)$ for three values of the correction parameter δ. The figure displays the corresponding ranges of allowed values of the 1PN tidal parameter $\bar{\alpha}_1$. Note that, for all models, the minima are rather shallow.

with $\bar{\alpha}_1 = 1.25$ and compute the corresponding χ^2 for the central value $\delta = 0.8$, we find that $\chi^2(\bar{\alpha}_2, 0.8)$ reaches a minimum around $\bar{\alpha}_2 \approx 40$. In addition the value of the minimum of the χ^2 is 3.20×10^{-7} which is slightly better than the performance of the 1PN Taylor model in the upper panel of Fig. 2. This shows again that higher-PN tidal effects can play an important role and that the minimima exhibited (for the central value $\delta = 0.8$) in the three panels of Fig. 2 should be viewed as effective values of $\bar{\alpha}_1$. We note in this respect that a situation where higher-PN corrections dominate over the 1PN one is not at all exceptional. For instance, the 1PN contribution to the EOB radial potential $A(r)$ *vanishes*; its 2PN contribution has a rather small coefficient, 2ν, while the numerical coefficient of the 3PN contribution νa_4 is quite large and significantly modifies the conclusions that one might draw from the first two PN contributions.

Further aspects of the comparison between numerical data and analytical models are illustrated in Figs. 3 and 4.

Figure 3 focuses on the 2B EOS model and contrasts (resummed) EOB (top panel) and (nonresummed) PN (bottom panel) analytical representations of the binding energy. In both cases, the NR binding energy is corrected by the same amount, namely, we assume that δ takes its central value $\delta = 0.8$. We see from this figure that the effect of the δ correction is comparable (in absolute value) to that of the added 1PN tidal contribution. Note that the value of the $\bar{\alpha}'_1$ parameter needed in the PN-expanded case (bottom panel) is significantly larger than the one needed in the EOB case (this was found to be true for all ways of modeling 1PN tidal contributions).

The χ^2 minima exhibited in Fig. 2 are at a similar level, $\chi^2_{\rm in} \approx 5 \times 10^{-7}$ (for all δ's in the range we considered), which corresponds to an average error level $\sqrt{\chi^2_{\rm min}/120} \approx 0.65 \times 10^{-4}$. The fact that this average error level is comparable to the virial error indicates that, all along the extended valley in the $(\bar{\alpha}_1, \delta)$ plane, shown in Fig. 2, there is an excellent agreement between the EOB predictions and the numerical data for *all* the EOS. (In view of Fig. 3 the same would hold for the NR/PN agreement, at the cost, however, of using, on average, significantly larger values of $\bar{\alpha}_1$.) As a particular illustration of the excellent possible NR/EOB agreement we exhibit in Fig. 4 the particular case $\delta = 1.2$ and $\bar{\alpha}_1 = 1.25$. By contrast to the central case $\delta = 0.8$ illustrated (for the 2B EOS) in Fig. 3 in which the (downward) δ correction was comparable to the (upward) effect of $\bar{\alpha}_1$, the more extreme $\delta = 1.2$ correction is here doing most of the work in bringing the NR data points down to the LO EOB level (which corresponds to the dashed line in the upper panel of Fig. 3.

Summarizing: the recent numerical data of Uryū *et al.* exhibit the influence of tidal interactions in close BNS systems. However, the presence of systematic errors in the data (due to an imperfect satisfaction of the helical-Killing-vector condition) partially masks the tidal interac-

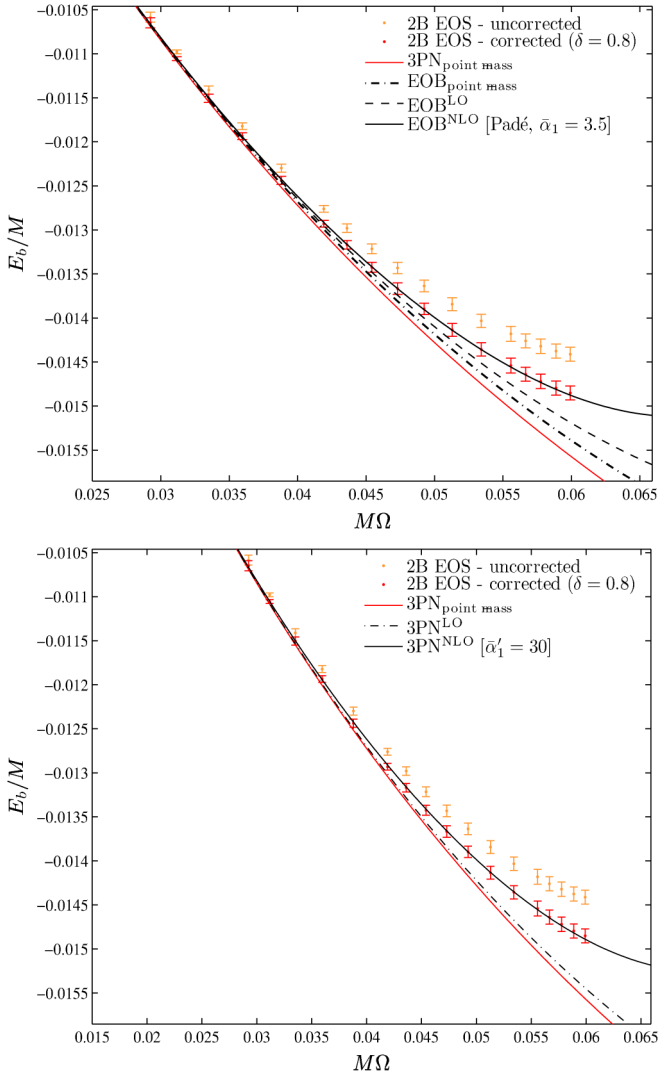

FIG. 3 (color online). Explicit comparison (for the 2B EOS) between various analytical representations of the binary binding energy and (corrected) numerical relativity data. The correction parameter is taken at its central value $\delta = 0.8$. The upper panel refers to EOB (resummed) models, and the lower panel to PN (nonresummed) models. For EOB^{NLO} effects, we use their Padé representation, Eq. (40) with $\bar{\alpha}_1 = 3.5$. For the $3PN^{NLO}$ model, we use $\bar{\alpha}'_1 = 30$.

tions and does not allow for a clean determination of the coefficients parametrizing tidal effects (and notably their 1PN contributions). The results of Fig. 1 suggest however that the NR data must be corrected by a term $\sim \delta x^4$ with $\delta \approx 0.8$. Then, this value of δ suggests the presence of significant higher-PN corrections that amplify the LO tidal effects.

We recommend that new nonconformally flat simulations be performed for several values of the radius r_0 at which the helical-Killing-vector condition is cut off. By studying the dependence of the results on r_0, it might be possible to extrapolate the results to an infinite value of r_0 (as used in analytical calculations), and thereby eliminate the 3PN-level systematic error δx^4.

V. INCORPORATING RADIATIVE TIDAL EFFECTS IN THE EOB FORMALISM

Besides the specific Hamiltonian (18) and (19), the other key ingredients of the EOB formalism are (i) a specific, factorized representation of the multipolar waveforms $h_{\ell m}$, and (ii) a resummed estimate of the radiation reaction force $\mathcal{F}$, which must be added to the conservative Hamiltonian dynamics (18) and (19). In the most recent, and seemingly most accurate, version of the EOB formalism the radiation reaction is analytically computed in terms of the multipolar waveforms. Therefore, it will be enough to estimate here the tidal correction to the multipolar waveforms $h_{\ell m}$. Following the factorization philosophy of Refs. [13,46,47] we shall look for tidal-correction factors $f^{\rm tidal}_{\ell m} = 1 + \mathcal{O}(\mu, \sigma)$, such that the EOB waveform would read

$$h_{\ell m} = f^{\rm tidal}_{\ell m} h^0_{\ell m}. \tag{63}$$

Here $h^0_{\ell m}$ is the factorized BBH EOB waveform, introduced in [46], and augmented by two next-to-quasi-circular parameters (a_1, a_2) in Ref. [1]. [Note, however, that, in view of the smallness of the tidal effects on the waveform, $f^{\rm tidal}_{\ell m} - 1 \ll 1$, it would be equivalent to use [as done for the $A(r)$ potential] an *additive* ansatz: $h_{\ell m} = h^0_{\ell m} + h^{\rm tidal}_{\ell m}$.]

In principle, one can use the effective action (4) and (5) to compute the tidal contributions to the waveform with any required relativistic accuracy (post-Minkowskian and/or post-Newtonian).

Here, we shall focus on the leading PN-order tidal correction to the leading PN waveform, i.e. the $\ell = 2, m = 2$ partial wave h_{22}. This will provide the leading tidal correction to the radiation reaction (which is predominantly given by a contribution $\propto |2\Omega h_{22}|^2$).

In that case, a shortcut for computing the tidal correction $f^{\rm tidal}_{22}$ consists of noting that the quadrupolar gravito-electric contribution in the action (4) corresponds to adding to the energy-momentum tensor of point masses an extra contribution $\Delta T^{\mu\nu}(x) \equiv 2g^{-1/2}\delta\Delta S_{\rm nonminimal}/\delta g_{\mu\nu}$, which describes the tidally induced quadrupole moment in each body A. At the leading Newtonian order this means that the quadrupole mass moment M_{ij} of the system will be

$$M_{ij} = \sum_A {\rm STF}_{ij}[M_A z^i_A z^j_A + \mu^A_2 G^A_{ij}], \tag{64}$$

where STF denotes a symmetric trace-free projection, and where the second term is the tidally induced quadrupole moment. Replacing the Newtonian value (8) of G^A_{ij} [computed using Eq. (9)] yields

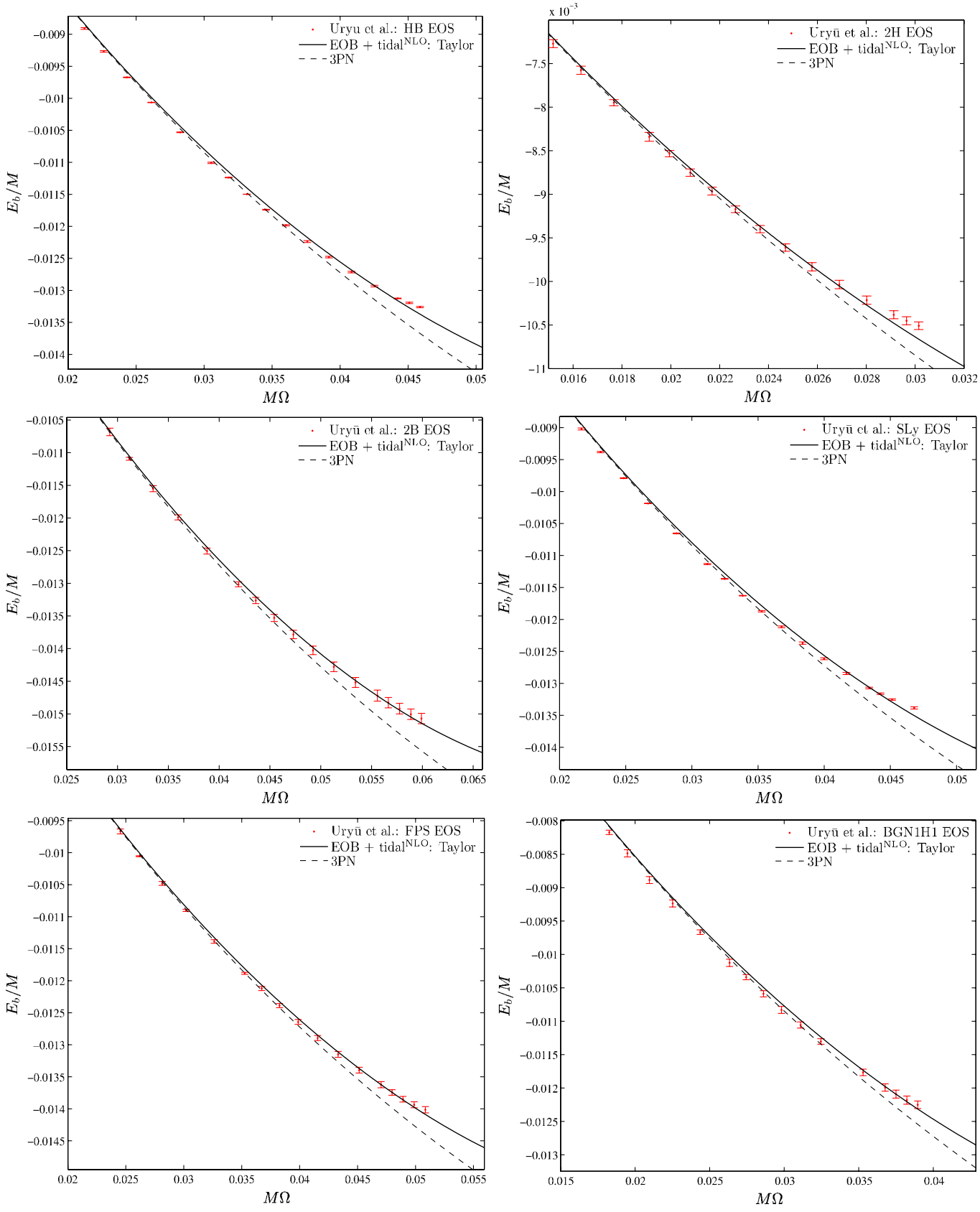

FIG. 4 (color online). Comparison between EOB^{NLO} predictions and NR binding energies for the six EOS of Table III. Here one uses the maximum acceptable value of δ (see lower-right panel of Fig. 1). The EOB description uses the analytically suggested value $\bar{\alpha}_1 = 1.25$ of the 1PN parameter and the linear NLO tidal model, Eq. (39). The 3PN point-mass curve is added to guide the eye.

$$M_{ij} = \sum_A \mathrm{STF}_{ij}\left[M_A z_A^i z_A^j + 3\mu_2^A G M_B \frac{z_{AB}^i z_{AB}^j}{r_{AB}^5} \right] = \left(\mu + \sum_A 3\mu_2^A \frac{GM_B}{r_{AB}^5} \right) r_{AB}^2 \hat{n}_{AB}^{ij}, \quad (65)$$

where $\mu \equiv M_A M_B/(M_A + M_B)$ is the reduced mass of the binary system, and where we reduced the first expression to the center-of-mass frame. Equation (65) agrees with Eq. (7) of [10] (in the limit where one neglects the excitation of the internal radial modes: $x_n \to 0$). In addition to the explicit tidal modification $\propto \mu_2^A$ that appears in the first factor of Eq. (65), there is an implicit tidal effect coming from the fact that the EOB waveform is conventionally expressed in terms of the (instantaneous) orbital frequency Ω of the binary system. We must then eliminate the relative distance r_{AB} in Eq. (65) in favor of Ω. This is done by using the adiabatic (quasicircular) Kepler law. The latter is modified by tidal forces:

$$\Omega^2 z_{AB}^i = -\frac{d^2 z_{AB}^i}{dt^2} = -\frac{1}{\mu}\frac{\partial L}{\partial z_{AB}^i} = \frac{GM}{r_{AB}^3} z_{AB}^i - \frac{1}{\mu}\frac{\partial L^{\mathrm{tidal}}}{\partial z_{AB}^i}. \quad (66)$$

Differentiating the leading ($\ell = 2$) tidal Lagrangian (16), and keeping only the leading ($\ell = 2$) term yields a modified Kepler law of the form

$$\Omega^2 r_{AB}^3 = GM\left[1 + 9\frac{M_B}{M_A}\frac{G\mu_2^A}{r_{AB}^5} + 9\frac{M_A}{M_B}\frac{G\mu_2^B}{r_{AB}^5} \right]. \quad (67)$$

Using (67) to solve r_{AB} in terms of Ω, and replacing the (tidally corrected) answer in (65) finally leads to a quadrupole moment of the form

$$M_{ij} = f_{22}^{\mathrm{tidal}} \mu r_{AB}^2 \hat{n}_{AB}^{ij} \quad (68)$$

with a tidal-correction factor

$$f_{22}^{\mathrm{tidal}} = 1 + \sum_A 3\frac{G\mu_2^A}{r_{AB}^5}\left(\frac{M_B}{\mu} + 2\frac{M_B}{M_A}\right) = 1 + \sum_A 3\frac{G\mu_2^A}{r_{AB}^5}\left(1 + 3\frac{M_B}{M_A}\right) = 1 + \sum_A 2k_2^A \left(\frac{R_A}{r_{AB}}\right)^5 \left(1 + 3\frac{M_B}{M_A}\right). \quad (69)$$

The factor f_{22}^{tidal} is the $\ell = 2$, $m = 2$ tidal-correction factor which was introduced in Eq. (63). It remains, however, to eliminate r_{AB} in terms of Ω, or, as used in the waveform of Ref. [46], in terms of the EOB variable $v_\Omega \equiv r_\Omega \Omega$ introduced in [48]: at the leading order it is enough to use $GM/c_0^2 r_{AB} = v_\Omega^2(1 + \mathcal{O}(1/c_0^2))$. This yields

$$f_{22}^{\mathrm{tidal}} = 1 + \left(\sum_A 2k_2^A \left(\frac{R_A c_0^2}{G(M_A + M_B)} \right)^5 \left(1 + 3\frac{M_B}{M_A} \right) \right) v_\Omega^{10}. \quad (70)$$

The result (70) agrees (after squaring it) with Eq. (8c) of Ref. [10] (in the limit $x_n \to 0$).

Summarizing: we propose to incorporate radiative tidal effects in the EOB formalism by inserting in the dominant $\ell = 2$, $m = 2$ waveform, a factor of the form

$$f_{22}^{\mathrm{tidal}} = 1 + \left(\sum_A 2k_2^A \left(\frac{R_A c_0^2}{G(M_A + M_B)} \right)^5 \left(1 + 3\frac{M_B}{M_A} \right) \right) \times v_\Omega^{10}(1 + \beta_1 v_\Omega^2), \quad (71)$$

where we included a possible 1PN correction to radiative tidal effects. One then computes a tidal-corrected radiation reaction by using this corrected waveform in the definition of $\mathcal{F}$ given in [13,46]. In principle the (mass-ratio dependent) coefficient β_1 can be computed analytically. It can also be calibrated by comparing NR data of inspiralling BNS systems to the EOB predictions.

VI. EOB PREDICTIONS FOR THE MOTION AND RADIATION OF INSPIRALLING COMPACT BINARIES

Having defined a specific EOB way of incorporating tidal effects in the motion and radiation of inspiralling compact binaries (BNS or BHNS) let us study the predictions made by the resulting tidally extended EOB formalism.

A. "Contact": A criterion for ending the EOB description

The EOB description of tidally interacting systems that we have introduced above assumes that the two considered objects (NS or BH) behave essentially as point masses. However, neutron stars are extended, and they are increasingly tidally distorted as they get near their companion. (This is also true for black holes, but their tidal distortion is much smaller; see below.) The issue of determining the moment when a neutron star is either too distorted to be treated as a point mass or even starts undergoing tidal disruption is a subtle one and is beyond the scope of this work. In the case of BHNS systems Ref. [49] has attempted to define an analytic indicator of the onset of tidal disruption [see their Eq. (30)] and has tried to delineate the domain of values of the mass ratio and the compactness for which tidal disruption was reached before encountering the last stable (circular) orbit (LSO).[6] Recent numerical works [50–52] have made considerable progress in simulating the dynamics of the merger of BHNS systems. However, it is difficult to extract from the numerical results a precise criterion for the eventual onset of tidal description. Leaving to future work a detailed comparison be-

[6]We note in passing that the fitting formula [their Eq. (33)] proposed in [49] for the orbital frequency at the innermost stable circular orbit is quantitatively quite different from the results obtained in the next section from our EOB approach.

tween the EOB description and numerical simulations of merging BNS and BHNS systems, we shall content ourselves here with a first cut at the problem of defining, within the EOB formalism, a criterion for ending the point-mass description phase of a BNS or BHNS system.

To orient our discussion, let us start by considering the dimensionless parameter controlling the tidal deformation of the NS labeled A by its companion B

$$\epsilon_A = \frac{M_B}{R^3}\frac{R_A^3}{M_A}. \tag{72}$$

We recall that it was found in [13] that the fractional deformation of the NS A is given by the product $h_2^A \epsilon_A$, where the shape Love number h_2^A is of order 0.8 for a typical NS compactness. Note, however, that the value of h_2^A computed in [13] corresponds to the situation where the external mass distorting the NS labeled A is located far away. In the case of the gravitational polarization of black holes by an external test mass, it was found in [53] (see Sec. 5 there) that the large separation shape Love number h_2 gets *amplified* by a separation-dependent factor $t_2(b)$ which increases as the separation decreases. The precise value of this amplification effect is not known in the case we are interested in, i.e., that of two comparable mass objects. We shall try to approximately take it into account by taking an effective shape Love number $h_2^{\rm eff} = 1$ (instead of 0.8).

The deformation parameter ϵ_A increases as the radial separation R between the two considered objects A and B decreases. The smallest possible value of R is given, in zeroth approximation, by the condition $R = R_A + R_B$, formally expressing that the two objects enter into contact (when B is a black hole we use simply[7] $R_B = 2GM_B/c_0^2$). Using this zeroth-order contact condition one can express the maximum value of ϵ_A in terms of the two compactnesses $c_A = GM_A/R_A$ and $c_B = GM_B/R_B$ as

$$\epsilon_A^{\rm contact_0} = \frac{c_B}{c_A}\frac{R_A^2 R_B}{(R_A + R_B)^3}. \tag{73}$$

For a symmetric, equal-mass BNS system, we see that, upon contact, $\epsilon_A^{\rm contact_0} = \epsilon_B^{\rm contact_0} = 1/8$. Then, using an effective shape Love number $h_2^{\rm eff} = 1$, we expect that, in a symmetric (or near symmetric) BNS system each NS is only deformed by about 12.5% at the moment of formal contact.

In the case of an asymmetric BNS system one can, however, obtain larger deformations. If, for instance, the label A denotes the NS having a larger radius, we will have $R_A > R_B$, and, correlatively, $M_A < M_B$ and $c_A < c_B$ (because of the properties of the mass-radius relation in neutron stars). Then, one finds that the rhs of Eq. (73) is *larger* than its symmetric value 1/8. For instance, if we consider for simplicity as EOS for the neutron stars a $\Gamma = 2$ polytrope, one finds that, for the extreme case where the mass ratio $M_A/M_B = 1/1.6$ one has $R_A/R_B \simeq 1.28$, and $8\epsilon_A^{\rm contact_0} \simeq 2.27$. In other words, using as above $h_2^{\rm eff} = 1$, the smaller-mass NS is now found to be deformed by about 28% at the moment of formal contact. This large value corresponds, however, to a NS having an astrophysically unrealistic small compactness $c_A = 0.0925$.

One can reach even larger deformations in the case of BHNS systems. If A labels the NS and B the BH, let us start by noticing that the dimensionless function $R_A^2 R_B/(R_A + R_B)^3$ (which depends only on the ratio R_A/R_B) reaches a maximum value of $2^2/3^3 = 4/27$ when $R_A = 2R_B$. As a consequence, we have the result

$$\epsilon_{A,\rm max}^{\rm contact_0} = \frac{4}{27}\frac{c_B}{c_A}. \tag{74}$$

In the present case, B denotes a BH (with $c_B = \frac{1}{2}$) so that

$$\epsilon_{A,\rm max}^{\rm contact_0} = \frac{2}{27 c_A} = \frac{0.074\,074}{c_A}. \tag{75}$$

Since NS compactnesses are expected to be larger than about 0.13, we find that, upon multiplication by $h_2^{\rm eff} = 1$, the NS in a BHNS system can be expected to be deformed by up to 57% at the moment of formal contact with its BH companion. Note that the reasoning above shows that such large deformations are only attained when $R_A = 2R_B$, i.e. when the mass ratio is equal to

$$\frac{M_B}{M_A} = \frac{c_B}{c_A}\frac{R_B}{R_A} = \frac{1}{2}\frac{c_B}{c_A} = \frac{1}{4c_A}. \tag{76}$$

For typical NS compactnesses $c_A \sim 0.15$, such a mass ratio $M_B/M_A \sim 1.67$ would correspond to a BH of a small mass ($M_B \sim 2.3M_\odot$ if $M_A \sim 1.4M_\odot$).

This preliminary analysis indicates that one can obtain very large distortions (probably quickly followed by tidal disruption) of the NS in the case of BHNS systems with a small mass ratio $M_B/M_A \sim 2$. This analytic finding is consistent with the results of recent numerical simulations [51,52]

In view of the large level of distortion that can occur in such systems, one can try to refine the zeroth-approximation definition of formal contact that we used above (to estimate $\epsilon_A^{\rm contact_0}$) by defining contact by the improved condition[8]

$$R = (1 + h_2^A \epsilon_A(R))R_A + (1 + h_2^B \epsilon_B(R))R_B, \tag{77}$$

[7] It is interesting to notice that in the case of an equal-mass BBH system the zeroth-approximation criterion for contact, $R = R_A + R_B = 2GM_A + 2GM_B = 2GM$, is in good agreement with the more sophisticated EOB definition of merger which consists of locating the maximum of the orbital frequency. See in this respect the penultimate row in Table III, which indicates the value $R^{\rm EOB\ merger} = 1.955GM$.

[8] We thank an anonymous referee for suggesting such an improvement.

TABLE III. EOB predictions for the characteristics of tidally interacting and near-merging binary systems (either BNS, BHNS, or BBH). These characteristics concern both the state of the systems at contact [in the sense of Eq. (77)] and at the last stable orbit. The EOB description is the NLO one of Eq. (43) with $\bar{\alpha}_1^{(\ell)} = 1.25$ and $\bar{\alpha}_2^{(\ell)} = 40$. The NS models are built using a $\Gamma = 2$ rest-mass polytropic EOS. From left to right, the columns report the type of binary, the name of the model (we use the same nomenclature as Refs. [54] for BNS and [52] for BHNS), the mass ratio $q = M_B/M_A$, the compactnesses c_A and c_B of the two objects, the values at contact of the tidal deformation parameters ϵ_A and ϵ_B, Eq. (72), the radial distance $R^{\rm contact}/GM$ (where $M = M_A + M_B$) at contact, twice the corresponding contact orbital frequency $2GM\Omega^{\rm contact}$, the adiabatic LSO radius $r_{\rm LSO}/GM$, and twice the corresponding adiabatic orbital frequency. In the case of BBH systems the contact properties refer to the EOB-determined moment of merger, i.e., the moment when the orbital frequency reaches a maximum.

Model	Name	q	c_A	c_B	$\epsilon_A^{\rm contact}$	$\epsilon_B^{\rm contact}$	$R^{\rm contact}/GM$	$2GM\Omega^{\rm contact}$	$R_{\rm LSO}/GM$	$2GM\Omega_{\rm LSO}^{\rm adiab}$
BNS	M3.6q1.00	1	0.13	0.13	0.0953	0.095 3	8.42	0.0832	7.235	0.108
BNS	M3.4q0.70	1.384	0.0871	0.172	0.196	0.035 2	9.245	0.0738	8.685	0.0832
BHNS	M20.145	2	0.145	0.5	0.474	0.005 78	3.714	0.230	5.412	0.159
BHNS	M20.160	2	0.160	0.5	0.467	0.007 65	3.384	0.248	5.184	0.167
BHNS	M30.145	3	0.145	0.5	0.546	0.01	3.041	0.252	5.246	0.164
BBH	⋯	1	0.5	0.5	⋯	⋯	1.955	0.352	4.619	0.193
BBH	⋯	∞	0.5	0.5	⋯	⋯	3.0	0.272	6.0	0.136

where $\epsilon_A(R)$ is the function of R defined in Eq. (72). Note that this condition defines $R^{\rm contact}$ only implicitly, as the rhs depends on R. In the case of NS's we shall take as shape Love numbers, h_2^A or h_2^B, the effective value $h_2^{\rm NSeff} = 1$. In the case where one of the two objects is a BH (say B), we shall take the (large distance) value $h_2^{\rm BH} = \frac{1}{4}$ derived in [53].

In Table III we list various quantities referring to the state of binary systems at the moment of contact as defined by the improved condition (77) (with $h_2^{\rm NS} = 1$ and $h_2^{\rm BH} = 1/4$). Here, we used as EOS for describing the NS interior a $\Gamma = 2$ rest-mass polytrope. In addition, we use here an EOB description which includes NLO effects in the tidal interaction energy. More precisely, we selected the 1PN + 2PN Taylor correction factor, Eq. (43), with $\bar{\alpha}_1^{(\ell)} = 1.25$ and $\bar{\alpha}_2^{(\ell)} = 40$. [Rigorously speaking the value $\bar{\alpha}_1^{(\ell)} = 1.25$ follows from Eq. (38) only when $\ell = 2$ and when considering an equal-mass system, and the value $\bar{\alpha}_1^{(\ell)} = 40$ was obtained by fitting equal-mass data. We use them anyway here, even for unequal-mass systems, as a semiquantitative example of the type of amplification factor implied by higher-PN tidal effects.]

We selected a small sample of representative systems: two BNS systems (with mass ratios 1 and 1.384), and three BHNS systems. We also included (for comparison purposes) two paradigmatic BBH systems. The two BNS systems considered here have been recently numerically simulated by Rezzolla *et al.* [54]. On the other hand, the three BHNS systems of Table III have been chosen among the ones recently simulated by Shibata *et al.* [52]. More precisely they correspond to the cases ($q = 2$, $c_A = 0.145$), ($q = 2$, $c_A = 0.160$), and ($q = 3$, $c = 0.145$). Among these systems, the simulations of [52] suggest that it is only for the first one, $q = 2$, $c_A = 0.145$, that the NS is disrupted in a way which creates, for a while, a significant torus ($M_{\rm torus}^{\rm baryon} \gtrsim 0.01 M_{\rm NS}^{\rm baryon}$) around the BH (see Figs. 4 and 7 in Ref. [52]).

It is interesting to note that our rather coarse description of the end of the inspiral phase is in rather good qualitative (and semiquantitative) agreement with the recent numerical relativity results. Indeed, in the case of BNS systems, the level of deformation of the largest (and lightest) NS (always labeled A) is in qualitative agreement with the recent results of [54] (see Figs. 1 and 2 therein, which correspond to our two selected cases). In the case of BHNS systems, we also seem to have good qualitative agreement with the results of [52]. In particular, note that in the case of $q = 2$, $c = 0.145$ the first panel of Fig. 4 of [52] suggests that the contact happens when the (coordinate) separation is $R^{\rm contact} \sim 4M$, with a quite large deformation. This is in semiquantitative agreement with our EOB description which predicts $R^{\rm contact} = 3.7M$, and $\epsilon_A^{\rm contact} = 0.47$. In the other BHNS cases, Table III predicts that contact occurs for a smaller radial separation, which is in qualitative agreement with, notably, Fig. 6 of [52]. It is physically clear that the value of $R^{\rm contact}/(GM)$ is crucial in determining the size of the formed torus. Only a relatively large $R^{\rm contact}/(GM)$, say large enough for a fraction of the mass of NS to be outside the LSO, is *a priori* expected to form a torus. Table III also contains information about the location of the LSO that will be discussed below.

Note also that (twice) the orbital frequency at contact is approximately given (if one uses the zeroth-approximation $R^{\rm contact} \approx R_A + R_B$ and Kepler's law) by the simple analytical formula

$$2GM\Omega^{\rm contact} \approx 2\left(\frac{X_A}{c_A} + \frac{X_B}{c_B}\right)^{-3/2}. \tag{78}$$

The main conclusion of this section is that the EOB formalism can consistently define, within itself, when one should

end the quasi-point-mass description of the binary inspiral. It can be approximately defined as the moment of contact between the two deformed objects, Eq. (77). We have found that in all cases of astrophysical interest (say $M_{\rm BH}/M_{\rm NS} \gtrsim 2$ and $c_{\rm NS} \gtrsim 0.13$) the analytically estimated deformation of the NS's was smaller than 55% at contact, which suggests that the NS has probably not yet been tidally disrupted in a well-detached state, but will start being disrupted just around the moment of formal contact. This tentative conclusion is preliminary because it is based on a rough description of contact and tidal distortion. [In particular, we evaluated the tidal distortion by using a shape Love number which is physically meaningful only for small deformations, and which was only minimally modified in an attempt to reflect the separation-dependent amplification factor $t_2(b)$ found in [53].] It seems, however, to be in semiquantitative agreement with recent numerical simulations. To refine our analytical approach [and notably for relating in a quantitative way $R^{\rm contact}/(GM)$ to the size of the torus formed by the subsequent disruption of the NS], it will be probably essential to compare in detail the EOB predictions to numerical simulations, and to improve our first-cut contact criterion, Eq. (77), by calibrating the effective values of the shape Love numbers h_2^A, h_2^B against numerical data.

B. Adiabatic inspiral and last stable orbit

Many previous works on binary systems involving NS studied the location of the LSO (also called innermost stable circular orbit, see e.g. Ref. [49]). In the case of BBH systems, the EOB approach predicted that the crossing of the LSO did not play a very important dynamical role, as there was a blurred, continuous transition between the early adiabatic quasicircular inspiral and the late nonadiabatic, but still approximately quasicircular, inspiral and plunge [33]. We similarly think that, in the case of BNS or BHNS systems, the crossing of the LSO does not play a crucial role in the orbital dynamics of the binary system. However, it is still interesting to know where it is located, and especially whether it occurs before or after (formal) contact. In addition, knowing the location of the LSO might be important for quantitatively discussing which fraction of the matter of a disrupted NS might form a relatively long-lived disk.

Let us then consider the *adiabatic* approximation to the inspiral, i.e. the approximation in which the inspiral is described as a sequence of circular orbits. It is indeed in this approximation that the concept of the LSO can be defined. We saw above the equation determining, in the EOB formalism, the sequence of circular orbits, Eq. (45). For large values of p_φ, and large values of r (i.e. small values of $u = 1/r$), Eq. (45) has a unique solution $r = 1/u \simeq p_\varphi^2$, corresponding to Newtonian circular orbits. However, when p_φ^2 decreases (as it does along the sequence of inspiralling orbits driven by radiation reaction), the sequence of stable circular orbits will terminate at certain values $r_{\rm LSO} \equiv 1/u_{\rm LSO}$, $p^2_{\varphi_{\rm LSO}}$ where there exists a double root of Eq. (45), i.e. a common root of Eq. (45) and

$$A''(u) + p_\varphi^2 B''(u) = 0. \tag{79}$$

The condition determining the radial location of the LSO is the vanishing of the determinant

$$\left| \begin{matrix} A' & B' \\ A'' & B'' \end{matrix} \right|_{\rm LSO} = A'(u_{\rm LSO})B''(u_{\rm LSO}) - A''(u_{\rm LSO})B'(u_{\rm LSO}) = 0. \tag{80}$$

For instance, in the test-mass limit, and in the absence of tidal corrections, i.e. for $A(u) = 1 - 2u$, $B(u) = u^2 A(u) = u^2 - 2u^3$, Eq. (80) reads $-4(1 - 6u_{\rm LSO}) = 0$, so that we recover the classic result $r_{\rm LSO} = 1/u_{\rm LSO} = 6$ (i.e. $r^{\rm phys}_{\rm LSO} = 6GM$) for the LSO around a Schwarzschild black hole. On the other hand, when inserting in Eq. (80) the complete value of the A function, i.e. the sum (22), where $A^0(r;\nu)$ is given by Eq. (21), and $A^{\rm tidal}(r)$ by Eq. (23), we see that the LSO predicted by the EOB formalism will depend both on the symmetric mass ratio ν, and on the EOB tidal constants κ_ℓ^T, Eq. (25). More precisely, these two types of effects (the ν-dependent ones which exist already in BBH systems, and the tidal-dependent ones which exist only in BHNS and BNS systems) act in opposite directions. Indeed, the ν-dependent contributions tend to make the radial potential $A(r)$ less attractive [see Eq. (20)], while the tidal ones make $A(r)$ more attractive. As a consequence, ν effects tend to move the radial location of the LSO toward smaller values [$r_{\rm LSO}(\nu) < 6GM$], while tidal effects tend to move $r_{\rm LSO}$ toward larger values. To avoid gauge effects, it is convenient to express the location of the (adiabatic) LSO in terms of the corresponding (real) orbital frequency

$$\Omega = \frac{\partial H_{\rm EOB}}{\partial p_\varphi^{\rm phys}} = \frac{1}{GM\mu} \frac{\partial H_{\rm EOB}}{\partial p_\varphi}. \tag{81}$$

Finally, we conclude that the dimensionless orbital frequency $GM\Omega$ at the LSO is a function of the dimensionless parameters ν, κ_ℓ^T which tends to increase as ν increases, and to decrease as κ_ℓ^T increases. We have seen above that the tidal coefficients κ_ℓ^T generically take rather large numerical values, of order $\kappa_2^T = \mathcal{O}(100)$, when $\ell = 2$; see Table I. However, they enter the A function at a higher order in u than the ν-dependent effects. As a consequence, the combination of the influences of ν and κ_2^T, κ_3^T, ... leads to orbital LSO frequencies which are sometimes larger, and sometimes smaller than the Schwarzschild value $GM\Omega_{\rm Schw} = 6^{-3/2} = 0.068\,04$. This is illustrated in Table III which lists the values of the LSO radial separation $R_{\rm LSO}/(GM)$, and of twice the orbital frequency (corresponding to the adiabatic gravitational wave frequency $\omega_{\ell m}$ for the dominant mode $\ell = m = 2$) for several paradigmatic systems: two BNS systems, three BHNS ones, and two BBH ones. If needed, one can convert the dimen-

sionless frequency $2GM\Omega$ in Hz by using $GM_\odot = 4.925\,490\,947\ \mu$s ($= 1.476\,625\,038$ km) so that the conversion factor between $\hat{\omega} = GM\omega$ and $f = \omega/2\pi$ is

$$f = \frac{\hat{\omega}}{2\pi GM} = 32.3125\hat{\omega}\left(\frac{M_\odot}{M}\right)\ \text{kHz}. \tag{82}$$

We see that, in the considered BNS systems, the LSO frequency is smaller than the Schwarzschild value $2GM\Omega_{\rm Schw} = 1/(3\sqrt{6}) = 0.136\,083$, and correspondingly, the radius of the LSO is larger than the canonical Schwarzschild $6GM$. [We found that one needed to consider BNS systems involving higher-compactness NS (approximately $c_A > 0.17$), to have an LSO frequency larger than the Schwarzschild value.] Note, by comparing BNS to BBH ones, how tidal effects can significantly change the LSO frequency by more than a factor of 2. In addition, note that, in BNS systems, contact occurs *before* the crossing of the LSO (so that the latter has no relevance). By contrast, in BHNS systems contact occurs *after* the crossing of the LSO. In other words the EOB predicts that, in BHNS systems, the NS will not be disrupted in a well-detached state (i.e., above the LSO), which would lead to the formation of a large torus.

Summarizing, the main conclusions of this section are that (i) the EOB formalism predicts that the quasi-point-mass description can be applied up to contact (where the tidal deformations can be large $\sim$50%, but not extremely large, i.e. $\sim$100%), without the possibility of disruption of the (lightest) NS in a well-detached state; (ii) the dimensionless orbital frequency at contact, $GM\Omega^{\rm contact}$, is significantly larger in BHNS systems (where $GM\Omega^{\rm contact} > GM\Omega_{\rm Schw} = 0.068\,04$) than in BNS systems (where $GM\Omega^{\rm contact} < GM\Omega_{\rm Schw}$); and (iii) the divide between the systems that cross the LSO before contact, and those that do not, depends strongly both on the composition of the system, on the compactnesses, and on currently unknown higher-PN corrections to tidal effects.

To end this section, let us mention that our results are *robust* under the choice of the EOB parameters a_5 and a_6 entering the BBH radial $A^0(r)$ potential, Eq. (21). The comparison between the currently most sophisticated version of the EOB formalism and the most accurate numerical relativity simulations has constrained the couple of parameters (a_5, a_6) to lie within a rather thin bananalike region in the (a_5, a_6) plane. We have checked that the results that we present in this paper are quite insensitive to the choice of a_5 and a_6 within this good region. The default values that we use in the present paper are $a_5 = -6.37$, $a_6 = +50$, which lie in the good region. To illustrate the insensitivity of our results to this choice, let us mention that the value of twice the orbital frequency at LSO, $2M\Omega^{\rm EOB}_{\rm LSO}(a_5, a_6)$ (for an equal-mass BNS system and for $c = 0.17$), changes from the value 0.136 05, to the new value 0.136 03 for $a_5 = -4$ and $a_6 = 24$ which lie near the upper boundary of the good region of parameters discussed in Ref. [1].

Note again that Table III was computed by assuming a specific (NR-tuned) 1PN + 2PN Taylor correction, Eq. (43). We illustrate in Table IV the dependence of our results on the choice of the NLO tidal-correction model. Table IV lists the same models and the same corresponding binary characteristics as Table III, but uses a different NLO tidal-correction model: specifically, it uses the 1PN-only model of Eq. (39) with the value $\bar{\alpha}_1^{(\ell)} = 7$, which was found to provide the best fit to the data of Ref. [15] when $\delta = 0.8$ (see Fig. 2). The comparison of the results of Table IV to those of Table III shows that (i) the characteristics at contact are quite robust under the change of the NLO model; (ii) on the other hand, the characteristics of the LSO are more sensitive to the choice of the NLO model. Note, in particular, that, in the case of unequal-mass BNS, the relative locations of the LSO and of contact are reversed. As, however, the location of the LSO does not have (within the EOB framework) any sharply defined physical meaning, these changes are probably of minor significance. This comparison therefore suggests that our physical predictions are robust under the change of the NLO model, when one considers two models tuned to the *same* NR data. On the other hand, one should keep in mind that the use of a *leading-order-only* tidal interaction would probably significantly affect the results listed in the tables.

Let us finally remark that the definition of contact used above relies on the use of the EOB radial coordinate. As this coordinate is a smooth deformation of the usual areal coordinate, we think that it is a reasonable definition to use as a first approximation. To refine it, it will be probably

TABLE IV. Same characteristics of binary systems as in Table III, but computed with $\bar{\alpha}_1^{(\ell)} = 7$ and $\bar{\alpha}_2^{(\ell)} = 0$.

Model	Name	q	c_A	c_B	$\epsilon_A^{\rm contact}$	$\epsilon_B^{\rm contact}$	$R^{\rm contact}/GM$	$2GM\Omega^{\rm contact}$	$R_{\rm LSO}/GM$	$2GM\Omega^{\rm adiab}_{\rm LSO}$
BNS	M3.6q1.00	1	0.13	0.13	0.0952	0.095 2	8.42	0.0834	7.789	0.0950
BNS	M3.4q0.70	1.384	0.0871	0.172	0.195	0.035 1	9.247	0.0739	9.318	0.0736
BHNS	M20.145	2	0.145	0.5	0.473	0.005 77	3.716	0.235	5.719	0.145
BHNS	M20.160	2	0.160	0.5	0.466	0.007 63	3.386	0.255	5.423	0.156
BHNS	M30.145	3	0.145	0.5	0.550	0.01	3.035	0.268	5.418	0.156
BBH	⋯	1	0.5	0.5	⋯	⋯	1.955	0.352	4.619	0.193
BBH	⋯	∞	0.5	0.5	⋯	⋯	3.0	0.272	6.0	0.136

necessary to compare in detail EOB predictions with results of NR simulations.

C. Phasing and waveform from the nonadiabatic inspiral of tidally interacting compact binaries

Let us now consider the motion and radiation of tidally interacting binaries predicted by the full EOB formalism, i.e. beyond the adiabatic approximation. This is obtained by integrating the EOB equations of motion

$$\frac{dr}{dt} = a(r)\frac{\partial \hat{H}_{\rm EOB}}{\partial p_{R_*}}, \qquad \frac{dp_{r_*}}{dt} = -a(r)\frac{\partial \hat{H}_{\rm EOB}}{\partial r}, \qquad \frac{d\varphi}{dt} = \frac{\partial \hat{H}_{\rm EOB}}{\partial p_\varphi}, \qquad \frac{dp_\varphi}{dt} = \hat{\mathcal{F}}_\varphi, \tag{83}$$

where $a(r) \equiv AD^{-1/2}$, $\hat{H}_{\rm EOB}(r, p_{r_*}, p\varphi) \equiv H_{\rm EOB}/\mu$, with $H_{\rm EOB}$ defined by Eq. (18), and where the (scaled) radiation reaction $\hat{\mathcal{F}}_\varphi = \mathcal{F}_\varphi/\mu$ is defined in the way introduced in [13] [see Eq. (3) there], i.e. by summing over ℓ and m the adiabatic multipolar partial fluxes corresponding to the newly resummed multipolar waves $h_{\ell m}$ [including the tidal correction (70) in h_{22}]. In addition, we recall that $r \equiv R/GM$, $t \equiv T/GM$, $p_\varphi \equiv P_\varphi/GM\mu$, and that the function $A(r)$ is here defined as the sum (22). Concerning the other metric coefficient $D^{-1}(r)$ [entering the auxiliary function $a \equiv (A/B)^{1/2} \equiv AD^{-1/2}$] we replace it by its standard resummation ($u \equiv 1/r$)

$$D^{-1}(r) = 1 + 6\nu u^2 + 2(26 - 3\nu)\nu u^3. \tag{84}$$

The solution of the ordinary differential equations (ODEs) (83) is then inserted in the newly resummed (and tidally completed) multipolar waves $h_{\ell m}$ to compute the waveform emitted by the inspiralling compact binary. Here, we shall focus on the $\ell = 2$, $m = 2$ dominant asymptotic waveform $\lim_{R\to\infty}(Rh_{22})$. Scaling it by $G\mu \equiv GM\nu$ and decomposing it in amplitude and phase,

$$\frac{R}{GM}\frac{h_{22}}{\nu} = A_{22}(t)e^{-i\phi_{22}(t)}, \tag{85}$$

we can then consider the dominant metric gravitational wave frequency $\omega_{22}(t) \equiv d\phi_{22}(t)/dt$. (Note that all these quantities are dimensionless. In particular, $\omega_{22} \equiv GM\omega_{22}^{\rm phys}$.)

Up to now we have discussed an extension of the EOB formalism which incorporates tidal effects in both the motion and the radiation of compact binaries. However, it has been advocated [10,12,44] to incorporate tidal effects as a modification of one of the nonresummed post-Newtonian-based ways of describing the dynamics of inspiralling binaries. In particular, the recent Ref. [12] uses as baseline a time-domain T4-type incorporation of tidal effects. To be precise, let us recall that the phasing of the T4 approximant is defined by the following ODEs:

$$\frac{d\phi_{22}^{\rm T4}}{dt} = 2x^{3/2}, \qquad \frac{dx}{dt} = \frac{64}{5}\nu x^5\{a_{3.5}^{\rm Taylor}(x) + a^{\rm tidal}(x)\}, \tag{86}$$

where $a_{3.5}^{\rm Taylor}$ is the PN-expanded expression describing point-mass contributions, given by[9]

$$\begin{aligned} a_{3.5}^{\rm Taylor}(x) = 1 &- \left(\frac{743}{336} + \frac{11}{4}\nu\right)x + 4\pi x^{3/2} + \left(\frac{34\,103}{18\,144} + \frac{13\,661}{2016}\nu + \frac{59}{18}\nu^2\right)x^2 - \left(\frac{4159}{672} + \frac{189}{8}\nu\right)\pi x^{5/2} \\ &+ \left[\frac{16\,447\,322\,263}{139\,708\,800} - \frac{1712}{105}\gamma - \frac{56\,198\,689}{217\,728}\nu + \frac{541}{896}\nu^2 - \frac{5605}{2592}\nu^3 + \frac{\pi^2}{48}(256 + 451\nu) - \frac{856}{105}\log(16x)\right]x^3 \\ &+ \left(-\frac{4415}{4032} + \frac{358\,675}{6048}\nu + \frac{91\,495}{1512}\nu^2\right)\pi x^{7/2}, \end{aligned} \tag{87}$$

and where $a^{\rm tidal}$ is given in the equal-mass case by [10]

$$a^{\rm tidal}(x) = 26\kappa_2^T x^5. \tag{88}$$

Here we shall analyze the (metric) GW phase ϕ_{22} as a function of the corresponding dimensionless frequency ω_{22} and study the influence on it of tidal effects. More precisely, we give here two different comparisons between the EOB predictions and the T4 one. In these two comparisons, we keep T4 unchanged and defined by Eq. (86), with a tidal contribution of the LO type (88). On the other hand, we compare this tidal-T4 model to two different tidal-EOB models; both models use a tidally modified A function, Eq. (22). One model ($\rm EOB^{LO}$) uses the LO $A^{\rm tidal}$, Eq. (23), while the other one ($\rm EOB^{NLO}$) uses the *Taylor* NLO $A^{\rm tidal}$, Eq. (39), with $\bar{\alpha}_1 = 7$. Here we consider a BNS equal-mass system modeled using the 2H EOS with compactness $c_A = c_B = 0.130\,97$, mass $M_A = M_B = 1.35M_\odot$, and radius $R_A = R_B = 15.23$ km.

The quantity which is plotted in Fig. 5 is the difference $\Delta\phi_{22}^{\rm EOBT4}(\omega_{22}) \equiv \phi_{22}^{\rm EOB^X}(\omega_{22}) - \phi_{22}^{\rm T4}(\omega_{22})$, where the label X on EOB takes two values, X = LO for the leading-order model and X = NLO for the next-to-leading-order model. To compute this quantity we took into account possible shifts in both $t(t^{\rm T4} = t^{\rm EOB} + \tau)$ and $\phi(\phi^{\rm T4} = \phi^{\rm EOB} + \alpha)$. We use here the two-frequency pinching technique of Ref. [56] to fix suitable values of the shifts τ and α. We use here two pinching frequencies which are close to 450 Hz. In other words, the phase

[9] We take this opportunity to mention that the expression of $a_{3.5}^{\rm Taylor}$ displayed in Appendix B of Ref. [55] contains two misprints: a missing $(59/18)\nu^2$ term in the coefficient of x^2 and an incorrect 452ν in the part of the coefficient of x^3 which is proportional to π^2. Note however that the equations used in our codes were correct.

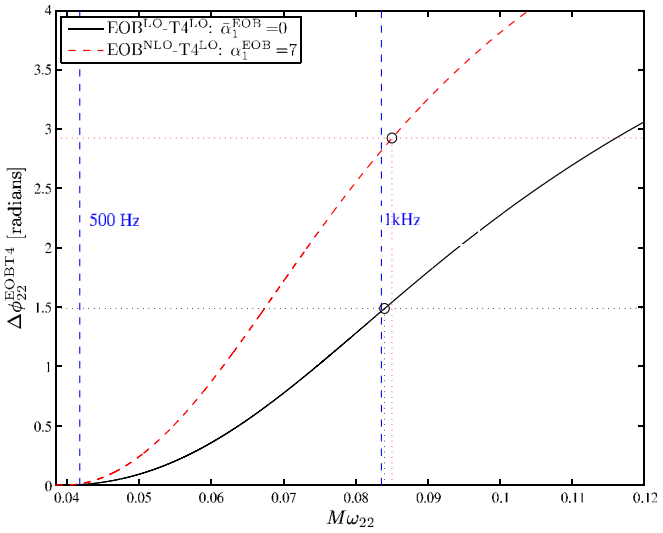

FIG. 5 (color online). Accumulated GW phase difference (versus the GW frequency ω_{22}) between two different tidal-EOB (quadrupolar) waveforms and a Taylor-T4-based PN waveform with (leading-order) tidal corrections, Eq. (86). The neutron star is modeled by a 2H EOS ($M = 1.35M_\odot$ and $c_A = c_B = 0.13097$). The two EOB models differ in the treatment of the NLO tidal effects: one uses only the leading-order tidal factor $\hat{A}_\ell^{\rm tidal} = 1$, while the other one uses Eq. (39) with $\bar{\alpha}_1^{(\ell)} = 7$. Waveforms have been suitably aligned (subtracting a relative time and phase shift) at low frequencies. The circles on the plot indicate, for each curve, the dephasing accumulated up to the contact frequencies.

differences displayed in our figure show the phase differences accumulated for frequencies between 450 Hz and the contact. Though, the figure does not display the phase differences below 450 Hz we have checked that they remain much smaller than what they become for frequencies higher than 450 Hz.

In Fig. 5, the solid black line displays $\Delta\phi_{22}^{\rm EOBT4}(\omega_{22}) = \phi_{22}^{\rm EOB^{LO}}(\omega_{22}) - \phi_{22}^{\rm T4}(\omega_{22})$, and the dashed red line $\Delta\phi_{22}^{\rm EOBT4}(\omega_{22}) = \phi_{22}^{\rm EOB^{NLO}}(\omega_{22}) - \phi_{22}^{\rm T4}(\omega_{22})$. The two circles on the curves indicate the final moments of contact [as defined using Eq. (77)]. We added two vertical dashed lines corresponding to 500 Hz and 1 kHz.

The main messages that one can draw from this figure are (i) the relative dephasing between EOB and T4 (using the same tidal model) grows by about 1.5 rad up to contact; (ii) the inclusion of higher-order PN-tidal contributions further increases the relative dephasing by nearly 1.5 rad more. Note that contact occurs just after the GW frequency reaches 1 kHz (which is within the sensitivity of some possible configurations of advanced LIGO). This indicates that the GW phasing of the ultimate part of the BNS inspiral is very sensitive to tidal effects and also very sensitive to their precise analytical modeling, including higher-order PN corrections. This makes it urgent to do high-accuracy comparisons between accurate NR simulations of BNS inspiral and EOB models, so as to accurately calibrate the EOB description of higher-order PN-tidal contributions.

VII. CONCLUSIONS

We discussed an extension of the EOB formalism which includes tidal effects. The hope is that such a tidal-EOB formalism will be able to go beyond the present PN-based proposals whose validity is limited to the early (lower-frequency) portion of the GW inspiral signal emitted by BNS systems. This formalism allows naturally for the presence of higher-order PN corrections to the leading (Newtonian) effects. We compared tidal-EOB predictions to recently computed numerical relativity data of quasiequilibrium circular BNS sequences [15]. We showed how to subtract tidal effects from NR data. Even after this subtraction, there remains a systematic difference between the ''point-mass'' NR binding energy and its EOB (and PN) analytical correspondent. We argue that this difference is due to unaccounted 3PN-level effects linked to the imperfect satisfaction of the helical-Killing-vector condition (which should be satisfied for physically waveless solutions). We advocate that new nonconformally flat simulations be performed for sequences of helical-Killing-vector cutoff radii so as to allow extrapolation to infinite radius. We also suggested to study BHNS circular binaries for mass ratios $M_{\rm BH}/M_{\rm NS}$ of order unity.

In absence of such physically waveless NR data, we proposed to subtract from the current data a term δx^4 representing a 3PN correction in the binding energy. We could then do a least-square analysis to try to minimize the (squared) distance χ^2 between NR data and tidal-EOB predictions. Our analysis allowed for 1PN corrections to tidal effects parametrized by $\bar{\alpha}_1$. We found that χ^2 remains close to its global minimum in a flat valley that extends over a significant region of the $(\bar{\alpha}_1, \delta)$ plane. This means that, given the present error level in numerical data, we cannot meaningfully and simultaneously select preferred values for $\bar{\alpha}_1$ and δ. Though this analysis is not fully conclusive, it does suggest the need of including higher-order PN correction to tidal effects that *significantly* increase their dynamical effect. [In other words, the effective value, say $\kappa_2^{\rm eff}(u) = \kappa_2^T(1 + \bar{\alpha}_1 u + \bar{\alpha}_2 u^2 + \cdots)$, which is relevant for the late inspiral is significantly larger, by a factor ~ 2, than κ_2^T.] These higher-order PN corrections might come not from the 1PN level, but from higher-PN levels (see, in particular, the end of Sec. IV, where a 2PN completion of a recently computed 1PN correction of order unity was shown to be fully compatible with current NR data).

This emphasizes the need both of higher-order analytical calculations of tidal effects and of high-accuracy numerical relativity simulations of inspiralling BNS systems. (We note in this respect that, when approximating a realistic tabulated EOS by a piecewise polytropic EOS, one should include an accurate description of the *low-density* EOS if

one wishes to accurately, and separately, reproduce the correct k_ℓ and radius; see, e.g., Table II in Ref. [42].) We argued that such a suitably tidally completed EOB formalism will be able to describe the dynamics (and GW emission) of inspiralling BNS or BHNS systems essentially up to the contact of the two objects. We emphasized that, though below the dimensionless (quadrupolar) GW frequency $GM\omega_{22} \sim 0.04$ (which corresponds to a frequency of 480 Hz for the $1.35M_\odot + 1.35M_\odot$ system), the present analytical knowledge is possibly sufficient for accurately describing the system, the GW phasing becomes uncertain by a large amount (~ 3 rad) during the late part of the inspiral, because of our current lack of secure knowledge of higher-order PN corrections to tidal effects. This makes it urgent to do high-accuracy comparisons between accurate NR simulation of BNS (or BHNS) inspiral and EOB models. These comparisons might be useful both ways: (i) in improving the EOB description, and (ii) in increasing our understanding of the tidal distortion and disruption, and of the possible formation of hot disks around merging systems. When the EOB description of higher-PN-tidal effects is ''calibrated'' with sufficient accuracy by using such EOB/NR comparisons, we think it will be possible to use the EOB formalism to extract from advanced-LIGO data some accurate knowledge of the nuclear EOS (via the measurement of the crucial parameter κ_2^T). Such an NR-calibrated EOB description might also be useful for delineating which systems are likely to generate sizable disks, and thereby short gamma-ray bursts.

ACKNOWLEDGMENTS

We are grateful to Loïc Villain for collaboration, at an early stage, on the NR-EOB comparison. We thank Koji Uryū for making available to us the numerical data behind the published tables of Ref. [15]. We are also grateful to Luca Baiotti, Bruno Giacomazzo, and Luciano Rezzolla for sharing with us, before publication, their data on inspiralling and coalescing binary neutron stars, which prompted our interest in relativistic tidal properties of neutron stars. We thank Ben Lackey for clarifying issues related to the piecewise polytropic description of realistic EOS. We also thank an anonymous referee for useful suggestions.

[1] T. Damour and A. Nagar, Phys. Rev. D **79**, 081503 (2009).
[2] A. Buonanno, Y. Pan, H. P. Pfeiffer, M. A. Scheel, L. T. Buchman, and L. E. Kidder, Phys. Rev. D **79**, 124028 (2009).
[3] N. Yunes, A. Buonanno, S. A. Hughes, M. C. Miller, and Y. Pan, arXiv:0909.4263 [Phys. Rev. Lett. (to be published)].
[4] L. Baiotti, B. Giacomazzo, and L. Rezzolla, Classical Quantum Gravity **26**, 114005 (2009).
[5] B. Giacomazzo, L. Rezzolla, and L. Baiotti, Mon. Not. R. Astron. Soc. **399**, L164 (2009).
[6] L. Baiotti, B. Giacomazzo, and L. Rezzolla, Phys. Rev. D **78**, 084033 (2008).
[7] L. Bildsten and C. Cutler, Astrophys. J. **400**, 175 (1992).
[8] C. S. Kochanek, Astrophys. J. **398**, 234 (1992).
[9] M. Vallisneri, Phys. Rev. Lett. **84**, 3519 (2000).
[10] E. E. Flanagan and T. Hinderer, Phys. Rev. D **77**, 021502 (2008).
[11] T. Hinderer, Astrophys. J. **677**, 1216 (2008).
[12] T. Hinderer, B. D. Lackey, R. N. Lang, and J. S. Read, arXiv:0911.3535.
[13] T. Damour and A. Nagar, Phys. Rev. D **80**, 084035 (2009).
[14] T. Binnington and E. Poisson, Phys. Rev. D **80**, 084018 (2009).
[15] K. Uryū, F. Limousin, J. L. Friedman, E. Gourgoulhon, and M. Shibata, Phys. Rev. D **80**, 124004 (2009).
[16] K. Uryū, F. Limousin, J. L. Friedman, E. Gourgoulhon, and M. Shibata, Phys. Rev. Lett. **97**, 171101 (2006).
[17] T. Damour, C. R. Acad. Sci. Paris, Sér. A **291**, 227 (1980).
[18] T. Damour, in *Gravitational Radiation*, edited by N. Deruelle and T. Piran (North-Holland, Amsterdam, 1983), p. 59.
[19] T. Damour, P. Jaranowski, and G. Schaefer, Phys. Lett. B **513**, 147 (2001).
[20] L. Blanchet, T. Damour, and G. Esposito-Farese, Phys. Rev. D **69**, 124007 (2004).
[21] L. Blanchet, T. Damour, G. Esposito-Farese, and B. R. Iyer, Phys. Rev. Lett. **93**, 091101 (2004).
[22] T. Damour and G. Esposito-Farese, Phys. Rev. D **53**, 5541 (1996).
[23] W. D. Goldberger and I. Z. Rothstein, Phys. Rev. D **73**, 104029 (2006).
[24] T. Damour and G. Esposito-Farese, Phys. Rev. D **58**, 042001 (1998).
[25] T. Damour, M. Soffel, and C. Xu, Phys. Rev. D **43**, 3273 (1991).
[26] T. Damour, Phys. Rev. D **81**, 024017 (2010).
[27] L. Blanchet and T. Damour, Phil. Trans. R. Soc. A **320**, 379 (1986).
[28] T. Damour, M. Soffel, and C. m. Xu, Phys. Rev. D **45**, 1017 (1992).
[29] T. Damour and G. Esposito-Farèse (unpublished).
[30] T. Damour, M. Soffel, and C. m. Xu, Phys. Rev. D **47**, 3124 (1993).
[31] T. Damour, M. Soffel, and C. m. Xu, Phys. Rev. D **49**, 618 (1994).
[32] A. Buonanno and T. Damour, Phys. Rev. D **59**, 084006 (1999).
[33] A. Buonanno and T. Damour, Phys. Rev. D **62**, 064015 (2000).
[34] T. Damour, Phys. Rev. D **64**, 124013 (2001).
[35] T. Damour and A. Nagar, arXiv:0906.1769.

[36] T. Mora and C. M. Will, Phys. Rev. D **69**, 104021 (2004); **71**, 129901(E) (2005).
[37] E. Berti, S. Iyer, and C. M. Will, Phys. Rev. D **77**, 024019 (2008).
[38] T. Damour, P. Jaranowski, and G. Schaefer, Phys. Rev. D **62**, 044024 (2000).
[39] T. Damour, P. Jaranowski, and G. Schaefer, Phys. Rev. D **62**, 084011 (2000).
[40] An old preprint by J. Isenberg, ''Waveless Approximation Theories of Gravity'' (University of Maryland, 1978), has been published recently: J. Isenberg, Int. J. Mod. Phys. D **17**, 265 (2008); J. Isenberg and J. Nester, in *General Relativity and Gravitation* edited by A. Held (Plenum Press, New York 1980), Vol. 1; Phys. Rev. D **65**, 044020 (2002); P. Grandclément, E. Gourgoulhon, and S. Bonazzola, Phys. Rev. D **65**, 044021 (2002).
[41] J. R. Wilson and G. J. Mathews, in *Frontiers in Numerical Relativity*, edited by C. R. Evans, L. S. Finn, and D. W. Hobill (Cambridge University Press, Cambridge, England, 1989), p. 306.
[42] J. S. Read, B. D. Lackey, B. J. Owen, and J. L. Friedman, Phys. Rev. D **79**, 124032 (2009).
[43] B. Lackey (private communication).
[44] J. S. Read, C. Markakis, M. Shibata, K. Uryū, J. D. E. Creighton, and J. L. Friedman, Phys. Rev. D **79**, 124033 (2009).
[45] P. Jaranowski and G. Schaefer, Phys. Rev. D **57**, 7274 (1998); **63**, 029902(E) (2000).
[46] T. Damour, B. R. Iyer, and A. Nagar, Phys. Rev. D **79**, 064004 (2009).
[47] T. Damour and A. Nagar, Phys. Rev. D **77**, 024043 (2008).
[48] T. Damour and A. Gopakumar, Phys. Rev. D **73**, 124006 (2006).
[49] K. Taniguchi, T. W. Baumgarte, J. A. Faber, and S. L. Shapiro, Phys. Rev. D **77**, 044003 (2008).
[50] Z. B. Etienne, J. A. Faber, Y. T. Liu, S. L. Shapiro, K. Taniguchi, and T. W. Baumgarte, Phys. Rev. D **77**, 084002 (2008).
[51] Z. B. Etienne, Y. T. Liu, S. L. Shapiro, and T. W. Baumgarte, Phys. Rev. D **79**, 044024 (2009).
[52] M. Shibata, K. Kyutoku, T. Yamamoto, and K. Taniguchi, Phys. Rev. D **79**, 044030 (2009).
[53] T. Damour and O. M. Lecian, Phys. Rev. D **80**, 044017 (2009).
[54] L. Rezzolla, L. Baiotti, B. Giacomazzo, D. Link, and J. A. Font, arXiv:1001.3074.
[55] T. Damour, A. Nagar, M. Hannam, S. Husa, and B. Bruegmann, Phys. Rev. D **78**, 044039 (2008).
[56] T. Damour, A. Nagar, E. N. Dorband, D. Pollney, and L. Rezzolla, Phys. Rev. D **77**, 084017 (2008).